

FMNEAR: determination of focal mechanism and first estimate of rupture directivity using near source records and a linear distribution of point sources

Bertrand Delouis

Géoazur, Université de Nice Sophia Antipolis, Observatoire de la Côte d'Azur, CNRS, 250 rue Albert Einstein, 06560 Valbonne delouis@geoazur.unice.fr

Supplemental Material is associated with this paper. It presents complementary information concerning the formulation of parameters, flow charts of the FMNEAR method, details about the computation of distance between focal mechanisms, waveform modelling of the majority of the test cases, results of the sensitivity tests, an example of waveform fit for inversions where the elimination of components as a function of waveform fit is disabled, and the crustal velocity models used.

Abstract

The FMNEAR method is based both on the waveform inversion of near-source seismic records and on a linear finite source model. The primary source parameters that are determined are the moment magnitude (M_w), the double couple focal mechanism (strike, dip, rake), and the distribution of seismic moment along strike, which provides a first order estimate of rupture length and directivity. Source depth is also explored. A specificity of the approach is the use of the finite source model directly within the search of the focal mechanism. This strategy allows the inclusion of strong motion records at short distances, for moderate to very large earthquakes ($M_w > 5.5$ to 9.0). However, for moderate to small earthquakes ($M_w < 5.5$) the source is simplified to a single point source. A specific band-pass filter is automatically adapted for each individual component of the seismograms (N, E, Z). The linear finite source is represented by point sources aligned along strike, each point source being characterized by a local source time function. The inversion is carried out in successive steps combining fast grid searches on the (strike, dip, rake) parameters and simulated annealing to determine rupture onset times and the shape of the local source time functions. The non-linear grid search offers the possibility of assessing the degree of uniqueness of the solution, and a confidence index is defined. The method was tested on eleven earthquakes worldwide, ranging in M_w from 4.5 to 9.0. Test cases incorporate continental events recorded by a large number of well-distributed stations and less favourable cases. In its present form, the FMNEAR approach is very well-adapted to continental earthquakes surrounded by seismic stations but it can also give informative results in more difficult configurations. The FMNEAR method is now ready for fully-automated determinations and is already implemented in near real-time.

Introduction

Inversion methods of the centroid seismic moment tensor (CMT) are routinely carried out at the global and regional scales (e.g., Global Centroid Moment Tensor catalogue [GCMT], Mediterranean Very Broadband Seismographic Network [MEDNET], National Research Institute for Earth Science and Disaster Prevention [NIED], Broadband Array in Taiwan for Seismology [BATS]; see Data and Resources section). Taking advantage of the linear relationship between the ground motion and the components of the seismic moment tensor, the latter can be obtained by fast linear inversion. However, without a proper consideration of the spatial extent of the rupture process, these methods are not well-adapted to the use of seismic records at distances smaller than several times the rupture length. Such records, hereafter called near source records, can only be used efficiently for large earthquakes if a finite dimension source model is considered. In contrast to regional and teleseismic broadband records, near source strong motion data are less commonly used for a rapid estimation of the source parameters of large earthquakes, even though they constitute the first records potentially available (short propagation time). Containing complementary waves, notably near-field waves, near source strong motion data bring a strong constraint on the source mechanism (e.g. Delouis and Legrand, 1999).

Our approach finds one of its nearest analogies in the work of Kuge (2003). This author analysed earthquakes in Japan of moment magnitude (M_w) ranging from 5.8 to 6.9, using strong motion records. In her approach, the point source and finite fault representations were successively employed in three steps, each solved by linear inversion. Firstly, the focal mechanism (moment tensor; hereafter called FM) was found using the point source approximation. Secondly, an alignment of point sources was used to test the two FM nodal planes that had been previously determined. Finally, a distribution of point sources on a rectangular finite fault model was considered. In the present work, we have used the same kind of data (strong motion records) and a similar linear source representation as described in Kuge (2003), but we intended to extend the magnitude range towards larger values by merging the first two steps previously described (Kuge, 2003), skipping the point source step. In our approach, the double couple FM is initially and directly determined using a linear distribution of point sources. The inversion is non-linear, but has the advantage that source finiteness is taken into account in the process of FM exploration. This is particularly needed for events with $M_w > 7$ if we want to use records at distances smaller than a hundred kilometres or so. We finish up with an FM determined by modelling the waveforms of the near-source records, a refined value of the seismic moment or M_w and we obtain information concerning rupture length and the distribution of seismic moment along the strike direction.

The extension of the method towards the production of automated 2D slip maps for the analysis of rectangular fault models will be addressed in future work. Assessing the robustness of such, more complex source models requires a specific calibration. Our present work focuses on primary source parameters: FM, M_w , first order rupture length and directivity, which are all crudely needed in the immediate post-event time-period and that may be obtained within a few tens of minutes, or less, depending on computing facilities. The results of this first linear source inversion can be also helpful in setting up subsequent more detailed finite-fault inversions. The fact that we do not propagate the rupture along dip will make identification of the actual rupture plane difficult in the case of dip-slip events, so the discrimination between the two nodal planes is not among our primary objectives here. Our method is particularly well-adapted for local networks installed in the source zone of potentially large earthquakes ($M_w > 7$). It is easily automated and has already been implemented in quasi-real-time in different seismological centres, including South-East France, Greece and Taiwan. For small earthquakes, it makes also use of broadband records.

The FMNEAR method

The epicenter and an initial estimate of the moment magnitude (hereafter called M_{wi}) are assumed to be known beforehand. In the application cases presented here, we will assume that the hypocenter depth may be less well-determined. Indeed, automated location systems are often based only on P waves, lacking the S waves to constrain the focal depth. Nevertheless, we will briefly address the specific question of the dependency of the FM solution, with possible errors, on the hypocenter location.

Data processing

An important part of the FMNEAR method is dedicated to data processing. This includes removing the pre-event baseline offset, picking the initial P wave arrival, doubly integrating the acceleration time series to obtain displacement, windowing, time shifting, band-pass filtering and decimation. For this paper, the first P arrival times were manually picked onto the vertical records to avoid mixing possible deficiencies coming from an automated picking algorithm and from the FMNEAR method itself. All other aspects of the data processing were automated and for a large part were performed using the SAC software package (see Data and Resources).

To be independent of the absolute timing of the time series, the observed signals are aligned with synthetic ones by computing the theoretical arrival time of the first P wave in the same 1D velocity model that is used to compute the synthetic seismograms. The alignment is performed by a simple time shift. Synthetic seismograms are computed using the discrete wave number method of Bouchon [1981] designed for one dimensional velocity models, and the theoretical arrival times are computed using the FASTHYPO program (Hermann, 1979). The window length for the waveform inversion is based on several factors. The hypocentral distance accounts for the propagation time, the magnitude of the event explains the rupture duration, and the lower boundary of the band-pass filter affects the time-frame of the window (the lower the low-cut frequency, the longer the window).

Filtering is a very important matter when dealing with the integration and waveform modelling of strong motion data. To study large earthquakes, we want to use as much as possible the low frequencies emitted by the rupture and contained in the seismograms. Most digital strong motion instruments theoretically offer the possibility to record frequencies down to that of static ground displacement. However, the occurrence of baseline shifts during strong shaking contaminates the signals and renders recovery of very long periods difficult (e.g. Iwan et al., 1985; Boore, 2001). To avoid contaminated low frequencies, an adapted high-pass filter has to be applied. We addressed this problem in detail in Delouis et al. (2009a), for the automated computation of M_w (MWSYNTH method) and here we use the same approach. Briefly, we analyse the acceleration spectrum of the whole seismic signal and identify deviations from the expected linear trend of the positive slope (near ω^2) at low frequency. The high-pass (i.e. low-cut) frequency (hereafter called f_{min}) is identified as the frequency from which the acceleration spectrum maintains a positive near constant slope up to the plateau area near the corner frequency.

The low-pass (i.e. high-cut) frequency (hereafter called f_{max}) is basically 3 times f_{min} but it is also constrained by magnitude and distance. We finish with boundary frequencies f_{min} and f_{max} , which define the filtering band-pass for individual components (North-South, East-West, and vertical). As a result, the bounding frequencies f_{min} and f_{max} are generally different for the three components of a same station. The signals are finally decimated to keep

only 8 points per shortest period ($1/f_{\max}$), a sampling rate that is a compromise between maintaining the waveforms and reducing computing time during inversion.

Determination of the FM parameters (strike, dip, rake)

The FM is explored using a two-step grid search. Each time a fault plane is tested (nodal plane defined by strike, dip, rake), a linear finite source model is inverted (Figure 1a). The source model orientation coincides with the strike of the plane (Figure 1b). The linear finite source model consists of a series of point sources, with an uneven number of points and an inter-point spacing scaled to M_{wi} . In practice, we estimate the rupture length from the relations of Wells and Coppersmith (1994), and point sources are distributed on a line measuring twice the estimated rupture length, with the middle point corresponding to the hypocenter. In this way, bilateral and unilateral ruptures can be explored. All point sources have the same depth. A local moment rate source time function (local STF) is associated to each point source, discretized by six mutually overlapping isosceles triangles. The width of the triangles is fixed according to M_{wi} . The onset time (rupture time, t_k in Figure 1a) of each point source, the rake angle and the amplitudes of the triangular elements are inverted for using a simulated annealing algorithm. The convergence criterion is the minimization of the normalized RMS misfit error on the waveforms, with a constraint aiming at minimizing also the total seismic moment. This procedure is taken from the multi-time-window kinematic source inversion of Delouis et al. (2002), except that here the source is linear, not rectangular, and the inversion is repeated for all the fault planes tested. Fixed parameters, and the value of M_{wi} from which they are derived, are presented in Table 2. The flow chart of the exploration scheme is presented in Figure S1, available in the electronic supplement to this article, but the different steps are described below.

Step 1, coarse search

In the first step of the grid search, we test 24 fault planes from 12 different FMs, 8 of which correspond to dip-slip and 4 to strike-slip solutions (Figure 2a). The rake angle may vary by $\pm 50^\circ$ around a central value. The strike, dip, and central rake values tested are shown in Figure 2a (top of beach balls). We test both nodal planes of the same FMs because the two planes will be associated with different oblique FMs when the rake angle is modified (Figure 2b). Overall, the 24 rupture planes, with their possible range of rake angles, correspond to distinct sub-areas in the parameter space, with only slightly overlapping common zones (there would be no overlap if the rake deviation were limited to $\pm 45^\circ$). This allows a rapid exploration of the whole parameter space of (strike, dip, rake), dividing it into sub-spaces and searching each sub-space independently.

Step 2, fine search

In the second step of the grid search, a refined exploration of the strike, dip and rake parameters is carried out. This is around the best solutions issued from both the previously tested dip-slip and strike-slip mechanisms. The two refined searches are needed because of the coarse character of the first step and also to provide a more uniform exploration of the parameter space needed to assess the uniqueness of the solution (confidence index, see below). First the strike is varied by $\pm 20^\circ$, then dip values of 15° , 30° , 45° , 60° , 75° are tested for the dip-slip case, and dip values of 60° , 75° and 90° are tested for the strike-slip case. Then the strike is varied again but only by $\pm 5^\circ$. Finally, the dip is varied again, by -10° , -5° , $+5^\circ$ and $+10^\circ$. At each sub-step, the exploration is conducted around the best solution previously found. A detailed flow chart of step 2 is shown in the electronic supplement to this article, Figure S2. During this refined exploration, each time a new doublet

(strike, dip) is tested the rake is inverted by the simulated annealing algorithm, within an interval of $\pm 30^\circ$ around the best rake value previously found.

Here, the FM is defined averaging the rakes of all the aligned point sources weighted by their respective seismic moment.

In total, 54 rupture planes are tested in steps 1 and 2 and stored with their corresponding RMS misfit function. This allows us to perform a review of the results in terms of their degree of uniqueness. Based on this analysis, a confidence index is computed (described below).

The RMS misfit function is normalized and corresponds to $RMS = \text{SQRT} [\sum w \cdot (\text{obs} - \text{cal})^2 / \sum w \cdot (\text{obs})^2]$ where SQRT is the square root, \sum is the sum over all data points from the seismograms, obs and cal the observed and calculated amplitudes respectively, and w is a weight which is normally 1, but which may be lower than 1 for stations located at short epicentral distances, and zero for discarded components (see below). The variance reduction in percent is $(1 - RMS) \times 100$. Without correlation, the use of a velocity model with an incorrect V_p/V_s ratio would produce large values of RMS misfits (large amplitude S and surface waves shifted), which in turn could lead to the rejection of a correct FM. Accordingly, we include the possibility of realigning the complete computed and observed signals using a cross-correlation during the inversion, with a maximum allowed time-shift of a few seconds (depending on the hypocentral distance).

Exploration of source depth

Due to limitations of computing time, we do not repeat the full inversion for different depths. Depth is only reassessed after a first run of the FM coarse search (step 1 as described above). A series of seven prescribed depths are tested, whose range depends on the initial depth. Depth is selected based on the RMS misfit criterion. Four additional depth values in the vicinity of this one are tested. The final depth is selected among the 12 tested depths (7 + 4 + initial). The coarse FM search is then redone with the final depth and step 2 (refined grid search) is carried out with this same depth. The depth values tested, which depend on the initial depth, can be found in the electronic supplement to this article.

Progressive discarding of erroneous and incorrectly modelled waveforms

During the inversion process, we identify station components whose waveforms are poorly matched and discard them. Successive thresholds in RMS misfit are considered. Thresholds 0.999 and 0.96 can be used in the case of poor data quality control before inversion, to remove first-order incorrect waveforms (erroneous interpretation of the amplitudes, out-of-order components etc.), which are mainly encountered in the case of (near) real-time application.

The main thresholds considered during the inversion are 0.85 and 0.65. Each time a threshold is observed, components whose RMS misfits lie above the threshold are discarded. Some inversion steps are then redone with the reduced dataset. Threshold 0.65 is only used after a first complete inversion, and then only if the confidence index is below 70%. In such a case, a new FM search is performed keeping only components whose RMS misfit is below 0.65 (see flow chart, Figure S1 available in the electronic supplement to this article).

This progressive procedure of data selection is justified notably, by the difficulty of automatically filtering strong motion records, which is generally affected by baseline shifts in acceleration, while aiming to preserve as much as possible the low frequencies. These last are necessary to constrain the source parameters of the largest earthquakes. This procedure

favours quality control in the perspective of a fully automated implementation, but it somehow reduces performance in terms of rapidity. A data quality control carried out before inversion will help to reduce the latter elimination of components. However, outliers in the FM inversion are not only related to problems in the data, they are also a consequence of the approximations and errors that have to be faced in the velocity model, in the source model, in the automated P wave picking and in the automated search for optimal filtering, as well as in the epicentre location. Accordingly, fully-automated inversion requires a higher level of, and more conservative, quality control based not only on the input data but also on the “a posteriori” criterion of data modelling. However, if the user wants to force the inversion to use all components, this can be readily implemented by modifying a parameter file (a choice included in the codes).

Underweighting of the nearest stations (distance < 20 kilometres)

Considering that there may be an error of a few kilometres as to the epicentre location and that such an error would imply strong variations in the travel path azimuth to the nearest stations, we incorporated a progressive reduction in the weight of stations nearer than 20kilometres (weight = [epicenter distance/20]², with a minimum weight of 0.1). This underweighting is also expected to help in cases where a significant slip variation occurs along dip in the vicinity of a station.

Assessing the quality of the inversion

We use three kinds of indicators to assess the quality of the results: (1) Comparison of computed FM, Mw, and moment distribution along strike with the published source models (reference); (2) Quality of the waveform modelling (RMS misfit function and visual comparison); (defined next) (3) A confidence index. Indicators (1) and (3) are the most important and they should be consistent, meaning that if the comparison with published results is poor, we expect a low confidence index.

The confidence index as defined here is an empirical indicator of the quality and uniqueness of the solution. It has been calibrated using a large database of events for which the FM has been independently determined. We take advantage of the exploration of the parameter space during the grid search steps. To obtain the confidence index we first compute the distance between the FM associated with the lowest RMS misfit function (i.e. the best solution) and all other 53 focal solutions explored.

To compute the distance between two FM solutions, we sample the focal hemisphere in azimuth and take-off angle, with a total of 324 points and compute the theoretical amplitude of the P wave for each FM at each of those points. The distance between two FM solutions is defined as the sum of the absolute value of the differences in P wave theoretical amplitude, predicted by the two mechanisms divided by the number of points that sample the focal hemisphere. This provides a distance of between 0 and 1, as illustrated in Figure S3 available in the electronic supplement to this article. Two FMs are hence considered similar if they predict similar amplitudes of the P wave over the focal sphere (in amplitude and sign).

Then we take into consideration the difference in RMS between the best solution and each of the others. The confidence index is built so that the index is low when a small RMS difference is associated with a large distance between FMs. Conversely, the confidence index is high in the absence of solutions associated with similar RMS and distant FMs.

As a result, the confidence index is based on the existence or not of secondary FM solutions that have an RMS misfit similar to that of the best solution but a very different FM. If such

secondary solutions exist, the confidence index is low, otherwise it is high. The confidence index also takes into consideration the intrinsic value of the best RMS value and the number of components used (the lower the RMS and the larger the number of components, the higher the confidence index). The confidence index is scaled between 0 (no confidence) and 100% (total confidence).

Examples of computed distances are shown in the Supplementary Material (Figure S3, available in the electronic supplement to this article). Figure 3 illustrates the distribution of solutions in graphs showing RMS versus FM distance from the inversions of the Chichi and Chengkung earthquakes, whose confidence indexes are 88% and 56%, respectively.

Test cases and results

We have applied the FMNEAR method to events that occurred in different tectonic settings and instrumental configurations. We selected events for which kinematic source inversions have been carried out using different datasets, so that we could compare the distribution of seismic moment provided by FMNEAR with the published slip distributions. First, we analysed three continental earthquakes that were well-surrounded by strong motion stations; Chichi in Taiwan (Mw 7.6), Tottori in Japan (Mw 6.7), and the L'Aquila in Italy (Mw 6.2). Then, we analysed two continental events for which the azimuth coverage of the stations is not so good: Chengkung in Taiwan (Mw 6.8) and Saintes in the French West Indies (Mw 6.3). Finally, to include larger events we considered subduction earthquakes, some being recorded by strong motion stations located above the rupture (Tarapaca (Mw 7.8) and Tocopilla (Mw 7.7), Chile), others located farther offshore (Miyagi-Oki (Mw 7.2), Tokachi-Oki (Mw 8.0) and Tohoku-Oki (Mw 9.0); Japan). In addition, to demonstrate that the method works well with small earthquakes, we included an event in France in 2006, located near the city of Lourdes (Mw 4.5). The earthquakes are described in Table 1.

For each earthquake we use a specific velocity model, generally taken from the literature for the area concerned. The velocity models are available in the electronic supplement to this article (Table S1).

The results of the source inversion are summarized in Table 3, and discussed below. We include a Figure for each test case, allowing a comparison between the FMNEAR focal solution and published FMs, as well as a comparison between simplified slip maps and the distribution of seismic moment along strike obtained with FMNEAR. Due to the large number of waveforms modelled, we show here the Figures for only a few cases, the other Figures being available in the electronic supplement to this article. Regarding slip maps, we selected results obtained from the joint inversion of various kinds of data, which generally guarantee a better constraint of slip distribution. We also intended to select models whose main features are representative of the overall published results.

Assessing rupture length is a delicate matter, given the one-dimensional rupture model used here to represent actual ruptures which may incorporate a large proportion of propagation along dip. However, to quantify and discuss this matter we define a threshold of 20% of the maximum seismic moment release (moment “peak”). Only point sources where seismic moment is above the threshold are considered in computing rupture length. We use also a threshold of 20% of maximum slip to define rupture length from the published slip maps.

Chichi earthquake (Mw 7.6)

The Chichi earthquake is one of the best instrumented events of the very large continental earthquakes. The FMNEAR FM is very similar to the published solutions (Figure 4), although

the rake suggests slightly more strike-slip movement. The distribution of seismic moment along strike indicates a maximum and a larger proportion of moment in the North, and a relatively low moment at the hypocenter, in agreement with the published slip maps. The dominant directivity towards the North is thus well-retrieved. Waveform fit is good overall (Figure 5), with signals dominated by periods of 30-40s. Rupture length is slightly overestimated by FMNEAR. The actual fault plane is selected as the best solution and the auxiliary plane is found with a difference (increase) in RMS of 0.06. This corresponds to a difference of 6% in the variance reduction between the actual and auxiliary planes, which means that the discrimination between the two nodal planes is not very robust.

Tottori earthquake (Mw 6.7)

The FM and the dominant propagation towards the SE are well-retrieved (Figure 6). Waveforms with dominant periods of around 20-30s are well-reproduced (Figure S4, available in the electronic supplement to this article). The estimated rupture length is correct. The actual fault plane is found as the best solution with a difference in RMS of 0.14 (14% of variance reduction) with respect to the auxiliary plane.

Aquila earthquake (Mw 6.3)

Again, the FM and the dominant direction of rupture directivity are well-retrieved (Figure 7), although the slip map suggests a larger portion of moment release towards the SE than the 45% found by FMNEAR. Waveform fit is good overall (Figure 8). We note however, that only one component (East) is retained for the closest stations AQU and AQG, and that the waveform fit is poor at station AQG. This can be related to the fact that stations at a distance smaller than 20 kilometres are down-weighted in the inversion (see above). Rupture length is slightly underestimated. The best solution corresponds to the auxiliary plane, but the real fault plane is found with a difference in RMS of only 0.04 (4% of variance reduction). This means that both nodal planes are approximately equivalent.

Chengkung earthquake (Mw 6.8)

The FM found is of the correct kind, although it is slightly rotated (more North-South, Figure 9). The distribution of seismic moment along strike is in disagreement with the slip map. Propagation to the North is overestimated and propagation to the South is underestimated. This may be due to the lack of seismic stations to the North of the epicenter. Waveforms are correctly matched (Figure S5, available in the electronic supplement to this article), but a relatively small proportion of components are finally retained (44%). Rupture length is slightly overestimated. The auxiliary plane is found as the best solution, the real one having an RMS difference of 0.06 (6% of variance reduction). The confidence index is low (56%) due to the existence of quite different FM solutions associated with similar RMS values (Figure 3).

Saintes earthquake (Mw 6.3)

The FM found is more strike-slip than the reference mechanisms, but the dominant normal component is well-retrieved (Figure 10). The seismic moment distribution reflects accurately the presence of the two slip patches on either sides of the hypocenter (bilateral propagation), with little slip at rupture initiation. Waveforms are nicely reproduced (Figure S6, available in the electronic supplement to this article) and rupture length is correctly assessed. The actual fault plane is selected as the best solution, although it is associated with an overestimated strike-slip component. The auxiliary plane appears with an RMS difference of 0.04 (4% of variance reduction), which means that the discrimination is not well-grounded.

Tarapaca earthquake (Mw 7.8)

The fault strike is rotated by 40° and the fault dip is overestimated by $15\text{-}25^\circ$ with respect to the reference solutions (Figure 11), but the general trend of the FM is reasonably well-retrieved. The rupture length is overestimated, but the seismic moment distribution indicates that most of it is located near the hypocenter, which is a good reflection of the condensed slip distribution. Waveform fit is presented in Figure S7 available in the electronic supplement to this article. The best solution corresponds to the actual fault plane, although the strike and dip are not very precisely retrieved. The auxiliary plane is associated with an RMS difference of 0.1 (10% of variance reduction).

Tocopilla earthquake (M_w 7.7)

The FM found lies very close to the reference solutions (Figure 12). The dominant propagation towards the South illustrated by the slip map is retrieved in the distribution of seismic moment along strike. Waveforms are dominated by 40-50s periods (Figure 13) and are very well-matched, especially at the closest stations. The rupture length is well-estimated. The actual fault plane is selected, with an auxiliary plane found with an RMS difference of 0.15 (15% of variance reduction).

Miyagi-Oki earthquake (M_w 7.2)

The FM is only approximately retrieved, with the fault strike rotated $20\text{-}40^\circ$, the fault dip overestimated by $25\text{-}30^\circ$ and the strike-slip component also overestimated (Figure 14). The seismic moment distribution along strike is nearly bilateral (47% towards the NE and 42% towards the SW), in relative agreement with the slip distribution. However, the slip distribution indicates mainly a down dip rupture propagation, a case which is not favourable for a linear source oriented along the fault strike. This may explain in part the moderate quality of the FM that was found. The waveform fit is shown in Figure S8, available in the electronic supplement to this article. A relatively small proportion of components are finally retained (49%). Rupture length is overestimated. The actual fault plane is selected as the best solution, but with the errors described above. The auxiliary plane is retrieved with an RMS difference of 0.06 (6% of variance reduction).

Tokachi-Oki earthquake (M_w 8.0)

The FM found is rotated $20\text{-}40^\circ$ in azimuth and the fault dip is overestimated by $25\text{-}35^\circ$, with respect to the reference solutions (Figure 15). The confidence index, rather low at 62%, reflects a relatively poorly constrained solution. The distribution of seismic moment indicates more moment towards the West, in partial agreement with the slip distribution that shows more slip to the South-West of the hypocentre. However, as in the case of the Miyagi-Oki earthquake, rupture propagation occurred mostly in the dip direction (slip map), a possibility not taken into account with the linear source considered here. The moderate quality of this determination may be related to the scarcity of seismic stations south of the epicenter (only one was considered). Waveform fit is displayed in Figure S9 available in the electronic supplement to this article. A small proportion of components are finally retained (29%), probably reflecting the relatively high degree of inadequacy of the rupture model. Rupture length is highly overestimated. The best solution is that closest to the actual fault plane, but the auxiliary plane is associated with an RMS difference of only 0.01 (1% of variance reduction), meaning that the model cannot really discriminate between the two nodal planes.

Tohoku-Oki earthquake (M_w 9.0)

The FM is well-retrieved in strike and faulting type, but the fault dip is overestimated by $35\text{-}45^\circ$ (Figure 16). The distribution of seismic moment indicates a strong concentration of moment immediately North and South of the hypocentre, displaying in total a rupture concentrated over about 300 kilometres along strike, in fair agreement with the slip model.

The waveform fit is not very good (Figure 17), with strong mismatches at several of the retained components, and with many components discarded (only 36% were retained). As for the two previously described earthquakes, this is likely to be related to the fact that an important portion of the rupture propagated in the dip direction, a possibility not taken into account by our linear source. However, given the proximity of the FM and moment distribution with the reference solutions, the high value of the confidence index, 87%, appears to be justified. With our criteria, rupture length is quite precisely retrieved. The actual fault plane with its overestimated dip is selected as the best solution, with an RMS difference of 0.06 (6% of variance reduction), relative to the auxiliary plane.

Near-Lourdes earthquake (M_w 4.5)

In the case of this much smaller event, the source is represented by a single point source at the hypocenter. The FM is in perfect agreement with the reference solutions (Figure 18), and the waveforms dominated by periods of 7-15s (Figure 19), are well-reproduced.

Running time

The present-day version of the codes is optimized to use a maximum of 7 CPUs simultaneously. Running time increases with magnitude (source parameters are increased), the number of stations, along with the distance of stations from the source, the maximum frequency (fmax), the complexity of the velocity model and the difficulty of finding a well-constrained solution (a second partial run is carried out if the confidence index after a first run is lower than 70%). Among the test cases presented here, running time on a Linux PC having 7 cores available was 1.5 minutes for Near-Lourdes, 10 minutes for L'Aquila, 11 minutes for Tocopilla, 46 minutes for Chichi and 1 hour for Tohoku-Oki. The codes could be better optimized, to use up to 24 CPUs simultaneously (this would be useful for the first step of the grid search).

Sensitivity tests

To assess the inversion sensitivity to the choice of stations and to the epicenter location, we carried out some tests with the Chichi earthquake using two subsets of 6 stations instead of 16 and displacing the Chichi epicentre 10 kilometres to the north (Figure S10, available in the electronic supplement to this article). We observed good stabilities of the M_w and FM. The spatial distribution of seismic moment exhibited more variation, although the dominant propagation towards the North was confirmed in all cases. We noted that the nodal plane chosen changed when the subset of stations was altered, confirming that the identification of the actual rupture plane is not a robust feature of this inversion approach, at least for dip-slip mechanisms. These simple tests are far from exhaustive, but they show that the results in terms of M_w , FM and main directivity have acceptable degrees of robustness with respect to the selection of stations and possible error as to the epicentre location.

We tested inversions in which the elimination of components associated with a lower waveform fit is disabled. Overall these led to lower confidence indexes, but results are barely modified. For example, Figure S11 (available in the electronic supplement to this article) shows the waveform fit in the case of the Chichi earthquake. The corresponding (strike, dip, rake) = (5, 30, 58) solution, with a confidence index of 84%, is very similar to that presented in Figures 4 and 5. However, the data of all the cases presented in this paper were subjected to visual inspection and off-line data quality control. This limited greatly the risk of erroneous data. In the case of real-time implementations, the selection of components on the basis of a good waveform fit provides a useful level of additional security.

For the Tohoku-Oki earthquake, we used the relocated epicenter (38.19N, 142.68E) identified by Chu et al. (2011). This differs significantly from the initial JMA-defined epicenter (38.103N, 142.861E). We also tested the performance of FMNEAR with the JMA epicentre (Figure S12 available in the electronic supplement to this article). The results are hardly affected by this change. Another problem concerning the Tohoku-Oki earthquake is the rapid and correct estimation of M_w , which is unusually large, to be used as the initial magnitude for FMNEAR. We tested FMNEAR with different values for the initial moment magnitude M_{wi} : 8.3, 8.5 and 8.7, instead of 9.0, to see if the final result depended on this initial value (Figure S12, available in the electronic supplement to this article). A significant underestimation of the initial M_w (8.3), led to an incorrect solution; that of a strike-slip mechanism associated with a relatively low confidence index (68%). A moderate underestimation of the initial M_w (8.5 or 8.7) led to acceptable solutions. We noted that the final M_w is dependent on the initial one, also being underestimated in these cases.

Near real-time implementation and testing

We implemented FMNEAR for testing in near real-time in Taiwan (Institute of Earth Sciences, Academia Sinica), Greece (National Observatory of Athens) and France (Géoazur laboratory). It was coupled to the MWSYNTH approach (Delouis et al., 2009a), which provides an initial M_w estimation. Earthquakes are detected and located by the monitoring system of the seismological observatory, then records are extracted in the SAC format, MWSYNTH is launched, and the resulting M_w is used as the initial M_w by FMNEAR which is run in fully automatic mode. To compute the FMs for regular seismicity, starting from a magnitude of 3.0-3.5, we also include the broadband velocity records in combination with strong-motion. The automated picking of the first P arrival is performed by the SAC “apk” picker (see Data and Resources section). Tests over several months (Greece) to a few years (Taiwan, France), show good convergence of solutions for moderate sized earthquakes ($3.5 < M_w < 6$), when determinations were obtained with different methodologies all based on the point source or centroid representation: BATS CMT, ISOLA, CAPS, TDMT for northern Italy – Southern France (see Data and Resources section). No large events ($M_w > 6.5$) have occurred to date in the areas where FMNEAR is presently tested in real-time. However, we expect FMNEAR to perform better than other local-regional methods in the case of large earthquakes, due to the use of the linear finite source.

Discussion and Conclusion

Overall, the main characteristics of the source are quite well-retrieved by the FMNEAR inversion. Nevertheless, we observe that the solution is affected by two main parameters: station coverage and propagation of rupture along dip.

Continental earthquakes with a good azimuthal distribution of stations are very satisfactorily resolved (Chichi, Tottori, Aquila). We show that a reduction in the number of stations (< 10) does not necessarily have a strong impact on the quality of the solution, provided the azimuthal coverage is not too much reduced (see tests with 6 stations for the Chichi earthquake). The rupture of a subduction earthquake occurring below the stations may also be well-resolved (e.g. Tocopilla). The solution may be impaired for earthquakes with poor azimuthal coverage, depending on the relative position of the stations with respect to the FM. In case of abatement, we expect the confidence index to decrease, providing the end-user with information about the unreliable nature of the solution.

Earthquakes for which a large part of rupture propagation is occurring along dip are less well-resolved by the along-strike linear source model. This could reflect a larger number of components being discarded, significant angular deviations in the FM and a tendency to

overestimate rupture length. This last effect is easily understandable, since slip propagation along dip is transferred in our model into slip along strike, the total seismic moment being more or less conserved. This is particularly the case for the Miyagi-Oki, Tokachi-Oki, Tohoku-Oki and Tarapaca earthquakes.

As mentioned above, the estimation of rupture length is a delicate matter since the definition of a threshold in the seismic moment distribution (here 20% of moment “peak”) is not strictly grounded. However, the quantification of the seismic moment proportion on both sides and at the level of the hypocenter provides a robust first-order indication of rupture directivity. The visual inspection of the distribution of seismic moment envelope is also interesting, to assess how concentrated or dispersed the rupture is. Only in one case, that of the Chengkung earthquake was rupture directivity found to be clearly wrong by FMNEAR. In that instance, the confidence index was low (56%). The difficulty in modelling that event may be related to the listric geometry of the rupture, as evidenced in Mozziconacci et al. (2009), and to the scarcity of seismic stations in the North.

The M_w retrieved from FMNEAR is to some extent dependent on the initial magnitude, but we observed a general tendency to underestimate M_w by 0.1 to 0.2 for large earthquakes (Table 3). Underestimation was strongest for the Tohoku-Oki earthquake (0.2 to 0.4). This observation may be explained at least partly by the fact that it is impossible to reproduce all the content of the waveforms with a simple linear source model. In the case of Tohoku, the main source area is located far offshore and strong motion stations may lose sensitivity to slip occurring near the trench.

By analysing the difference in RMS misfit (or variance reduction) between the solutions closest to the actual and auxiliary planes, we could see that discrimination between the two nodal planes of dip-slip FMs is not generally possible with the linear source model. In three cases, the auxiliary plane is even chosen as the best solution. Only in the cases of Tottori and Tocopilla, and to some extent Tarapaca, is the discrimination quite clear, with greater than 10% difference in variance reduction. Tottori is the only strike-slip event and a good discrimination was expected for this earthquake, since the line source models associated with the two nodal planes are perpendicular, i.e. very distinct.

We hardly comment the final depth found by FMNEAR, since this is dependent on the choice of the velocity model, and also because the reference depth is not always well constrained. However, we note a significant difference between the inverted and reference depths for the Tottori, Tokachi-Oki, and Tohoku-Oki earthquakes. The performance of the FMNEAR method could be improved when focalizing on a specific region, by taking into account velocity models that are optimized for that area. Such optimization was beyond the objectives of this rather general study.

From the analysis of the results presented here, and additional cases where FMNEAR has been implemented for routine determinations, we conclude that solutions with a confidence index smaller than 70% should be considered with caution. Above 80% confidence, results are in general very well-established. Nevertheless, a visual inspection of the waveform fits remains a good complement to assess the quality of the solution.

Discarding components on the basis of a threshold in waveform fit may produce a loss of information in some cases, but it provides protection against potential inadequacies in different aspects of the model (Earth structure, source etc.), possible failures in the initial data quality control, especially for (near) real-time implementations, and modelling errors due to

the use of a simple source representation. In cases where the user has a great confidence in the quality of the data and in the Earth model, he may choose to keep all the components.

Along the Japan Trench, earthquakes seem to involve somewhat systematically a large, or even dominant, portion of propagation along dip (e.g. Miyagi-Oki, Tokachi-Oki). The mega Tohoku-Oki earthquake, although shallower than the other two events, produced a rupture of unexpectedly short dimension along strike. Its low length/width ratio is particularly clear when compared to the 2004 Giant Sumatra earthquake. Accordingly, a specific strategy may be necessary for studies pertaining to this region, such as the use of bilinear finite source models with a line shorter than that presently used along strike and a second perpendicular line along dip. This will be the subject of a further report. However, for continental areas, where the rupture width is limited by the seismogenic thickness of the crust, the FMNEAR method in its present form should provide good results, even for the largest earthquakes. Indeed, we demonstrate that FMNEAR can resolve the first order source parameters (M_w , FM) over a very large range of magnitude (4.5 to 9.0 in the examples shown here) and that it can provide meaningful information about directivity for large events.

Data and Resources

Earthquake data (location, reference moment magnitude, strong-motion records) were obtained either from published studies (see reference list) or from diverse institutions whose acronyms are explicated below. Also described, various acronyms corresponding to organisms publishing source parameters and to methods of source inversion. BATS: Broadband Array in Taiwan for Seismology <http://bats.earth.sinica.edu.tw/> (last accessed April 2013). CAP: “Cut and Paste” waveform inversion by Zhu and Helmberger (1996). CWB: Central Weather Bureau, Taiwan, <http://www.cwb.gov.tw/eng/index.htm> (last accessed May 2013). GCMT: Global Centroid Moment Tensor catalog, www.globalcmt.org/CMTsearch.html (last accessed April 2013). K-NET: Kyoshin Network, accelerometric data, Japan. <http://www.kyoshin.bosai.go.jp> (last accessed May 2013). IGN: Instituto Geográfico Nacional, Spain, <http://www.ign.es/ign/layoutIn/sismoDetalleTerremotos.do?evid=1060340&zona=1> (last accessed May 2013). INGV: Istituto Nazionale di Geofisica e Vulcanologia, Italy, <http://www.ingv.it/en> (last accessed May 2013). ISOLA: Retrieve Isolated Asperities from Regional or Local Waveforms, by J. Zahradnik and E. Sokos, <http://seismo.geology.upatras.gr/isola> (last accessed April 2013). ITACA: national strong motion network (“Rete Accelerometrica Nazionale”, RAN) managed by the Italian Civil Protection, <http://itaca.mi.ingv.it/ItacaNet> (last accessed May 2013). JMA: Japan Meteorological Agency, Japan, <http://www.jma.go.jp/jma/indexe.html> (last accessed May 2013). MEDNET: Mediterranean Very Broadband Seismographic Network, by Pondrelli et al. (2006), <http://mednet.rm.ingv.it/rcmt.php> (last accessed April 2013). NIED: National Research Institute for Earth Science and Disaster Prevention, <http://www.bosai.go.jp/e/index.html> and http://www.hinet.bosai.go.jp/AQUA/aqua_catalogue.php?LANG=en (last accessed April 2013). RAP: Réseau accélérométrique permanent, French accelerometric network, <http://www-rap.obs.ujf-grenoble.fr/> (last accessed May 2013). RAGIC: joint accelerometric network of the Geophysics and Civil Engineering departments of the University of Chile. Records were retrieved from the now inactive webpage <http://www.ingcivil.uchile.cl>. Data are now made available via <http://terremotos.ing.uchile.cl/> (last accessed May 2013). SCARDEC: rapid determination of seismic moment magnitude, focal mechanism and source time functions for large earthquakes using body wave deconvolution (Vallée et al., 2011), <https://geoazur.oca.eu/spip.php?article1236> (last accessed May 2013). TDMT: Time

Domain Centroid Moment Tensor inversion (ref. Dreger, 2003) <ftp://www.orfeus-eu.org/pub/software/iaspei2003/8511.html> (last accessed April 2013), TDMT-INGV implemented for Italy <http://cnt.rm.ingv.it/tdmt.html> (last accessed April 2013). USGS W-phase CMT, <http://earthquake.usgs.gov/earthquakes> (last accessed May 2013)/

Some Figures were partly made using GMT (Generic Mapping Tools) package by Wessel and Smith (www.soest.hawaii.edu/gmt, last accessed April 2013)

Seismic data processing was partly done using the SAC (Seismic Analysis Code) package by Peter Goldstein (<http://www.iris.edu/software/sac/sac.request.htm>, last accessed April 2013)

Acknowledgement

This work was carried out in the framework and under the support of the European Community - NERA (Network of European Research Infrastructures for Earthquake Risk Assessment and Mitigation) project. I am grateful to the two anonymous reviewers who helped improving the manuscript.

References

- Boore, D. M. (2001). Effect of baseline corrections on displacement and response spectra for several recordings of the 1999 Chi-Chi, Taiwan, earthquake, *Bull. Seism. Soc. Am.* 91, 1199-1211.
- Bouchon, M. (1981). A simple method to calculate Green's functions for elastic layered Media, *Bull. Seism. Soc. Am.*, 71 (4), 959-971.
- Chang, C. H., Y. M. Wu, T. C. Shin, and C. Y. Wang (2000). Relocation of the 1999 Chi-Chi Earthquake in Taiwan, *Terr. Atmos. Oceanic Sci.*, Vol. 11, No. 3, 581-590
- Chu, R. S., W., Helmberger, D.V., Zhan, Z., Zhu, L., and H. Kanamori (2011). Initiation of the great Mw 9.0 Tohoku-Oki earthquake, *Earth Planet. Sci. Lett.* 308, 277-283.
- Cirella, A., A. Piatanesi, M. Cocco, E. Tinti, L. Scognamiglio, A. Michelini, A. Lomax, and E. Boschi (2009). Rupture history of the 2009 L'Aquila (Italy) earthquake from non-linear joint inversion of strong motion and GPS data, *Geophys. Res. Lett.*, 36, L19304, doi:10.1029/2009GL039795.
- Delouis, B. and D. Legrand (1999). Focal mechanism determination and identification of the fault plane of earthquakes using only one or two near-source seismic recordings. *Bull. Seism. Soc. Am. Bulletin* 89, 1558–1574.
- Delouis, B., D. Giardini, P. Lundgren, and J., Salichon (2002). Joint inversion of InSAR, GPS, teleseismic and strong motion data for the spatial and temporal distribution of earthquake slip: Application to the 1999 Izmit Mainshock, *Bull. Seism. Soc. Am.*, 92, 278-299.
- Delouis, B. and D. Legrand (2007). The Mw 7.8 Tarapaca intermediate depth earthquake of 13 June 2005 (northern Chile): Fault plane identification and slip distribution by waveform inversion, *Geophysical Research Letters*, 34, L01304, doi:10.1029/2006GL028193.
- Delouis, B., J. Charlety, and M. Vallée (2009a). A method for rapid determination of moment magnitude Mw for moderate to large earthquakes from the near-field spectra of strong-motion records (MWSYNTH), *Bull. Seismol. Soc. Am.* 99, no. 3, 1827–1840, doi 10.1785/0120080234.
- Delouis, B., M. Pardo, D. Legrand, and T. Monfret (2009b). The Mw 7.7 Tocopilla earthquake of 14 November 2007 at the southern edge of the northern Chile seismic Gap: Rupture in the deep part of the coupled plate interface, *Bull. Seism. Soc. Am.*, 99, 87-94, doi: 10.1785/0120080192.

- Dreger, D. S. (2003). TDMT_INV: Time Domain Seismic Moment Tensor INVersion, *International Handbook of Earthquake and Engineering Seismology*, Volume 81B, p 1627.
- Feuillet, N., Beauducel, F., Jacques, E., Tapponnier, P., Delouis, B., Bazin, S., Vallée, M., and G.C.P. King (2011). The Mw = 6.3, November 21, 2004, Les Saintes earthquake (Guadeloupe): Tectonic setting, slip model and static stress changes, *J. Geophys. Res.*, 116, B10301, doi:10.1029/2011JB008310.
- Herman, R.B. (1979). FASTHYPO - a hypocenter location program, *Earthquake Notes*, 50, 2.
- Iwan, W. D., M. A. Moser, and C. Y. Peng (1985). Some observations on strong-motion earthquake measurement using a digital accelerograph, *Bull. Seism. Soc. Am.* 75, 1225-1246.
- Iwata, T., and H. Sekiguchi (2002), Source process and near-source ground motion during the 2000 Tottori-ken Seibu earthquake, paper presented at 11th Japan Earthquake Engineering Symposium, *Earthquake Eng. Res. Liaison Comm.*, Sci. Coun. of Japan., Tokyo
- Ji, C., D. V. Helmberger, D. J. Wald, and K. F. Ma (2003). Slip history and dynamic implications of the 1999 Chi-Chi, Taiwan, earthquake, *J. Geophys. Res.*, 108, (B9), 2412, doi:10.1029/2002JB001764, 2003
- Kuge, K (2003). Source modeling using strong-motion waveforms: Toward automated determination of earthquake fault planes and moment-release distributions, *Bull. Seism. Soc. Am.*, 93, 639-654.
- Kuoehen, H., Wu, Y.M., Chen, Y.G. & Chen, R.Y. (2007). Mw6.8 Chengkung earthquake and its associated seismogenic structures, *J. Asian Earth Sci.*, 31, 332–339.
- Ma, K.-F., E. E. Brodsky, J. Mori, C. Ji, T.-R. A. Song, and H. Kanamori (2003), Evidence for fault lubrication during the 1999 Chi-Chi, Taiwan, earthquake (Mw7.6), *Geophys. Res. Lett.*, 30, 1244, doi:10.1029/2002GL015380, 5.
- Mozziconacci, L., B. Delouis, J. Angelier, J. C. Hu, and B. S. Huang (2009). Slip distribution on a thrust fault at a plate boundary: the 2003 Chengkung earthquake, Taiwan, *Geophys. J. Int.*, 177, 2, 609-623, DOI: 10.1111/j.1365-246X.2009.04097.
- Ohmi, S., Watanabe, K., Shibutani, T., Hirano, N., and S. Nakao (2002). The 2000 Western Tottori Earthquake—Seismic activity revealed by the regional seismic networks, *Earth Planets Space*, 54, 819–830.
- Pondrelli, S., S. Salimbeni, G. Ekström, A. Morelli, P. Gasperini and G. Vannucci, (2006). The Italian CMT dataset from 1977 to the present, *Phys. Earth Planet. Int.*, doi:10.1016/j.pepi.2006.07.008, 159/3-4, pp. 286-303, 2006.
- Semmane, F., F Cotton, and. M Campillo (2005). The 2000 Tottori earthquake: A shallow earthquake with no surface rupture and slip properties controlled by depth – *J. Geophys. Res.*, vol. 110, B03306, doi:10.1029/2004JB003194
- Sylvander, M., Souriau, A., Rigo, A., Tocheport, A., Toutain, J.-P., Ponsolles, C. and S. Benahmed (2008), The 2006 November, ML= 5.0 earthquake near Lourdes (France): new evidence for NS extension across the Pyrenees. *Geophys. J. Int.*, 175: 649–664. doi: 10.1111/j.1365-246X.2008.03911.x
- Vallée, M., J. Charléty, A.M.G. Ferreira, B. Delouis, and J. Vergoz (2011). SCARDEC : a new technique for the rapid determination of seismic moment magnitude, focal mechanism and source time functions for large earthquakes using body wave deconvolution, *Geophys. J. Int.*, 184, 338-358.
- Wells, D. L., and K. J. Coppersmith (1994). New empirical relationships among magnitude, rupture length, rupture width, rupture area, and surface displacement, *Bull Seism. Soc. Am.* 84, 974-1002.
- Wu, C., K. Koketsu, and H. Miyake (2008), Source processes of the 1978 and 2005 Miyagi-oki, Japan, earthquakes: Repeated rupture of asperities over successive large earthquakes, *J. Geophys. Res.*, 113, B08316, doi:10.1029/2007JB005189.

- Wu, Y.-M., Y. G. Chen, T. C. Shin, H. Kuochen, C. S. Hou, J. C. Hu, C. H. Chang, C. F. Wu, and T. L. Teng (2006), Coseismic versus interseismic ground deformations, fault rupture inversion and segmentation revealed by 2003 Mw 6.8 Chengkung earthquake in eastern Taiwan, *Geophys. Res. Lett.*, 33, L02312, doi:10.1029/2005GL024711.
- Yagi, Y., and M. Kikuchi (1999) Preliminary results of rupture process for the September 21, 1999 Chi-Chi Earthquake, <http://www.eic.eri.utokyo.ac.jp/yuji/taiwan/taiwan.html> (last accessed May 2013).
- Yagi, Y. (2004). Source rupture process of the 2003 Tokachi-oki earthquake determined by joint inversion of teleseismic body wave and strong ground motion data, *Earth Planets Space*, 56, 311–316.
- Yamanaka, K. and M. Kikuchi (2003). Source processes of the Tokachi-oki earthquake on September 26, 2003, inferred from teleseismic body waves, *Earth Planets Space*, 55, e21–e24, 2003.
- Yokota, Y., K. Koketsu, Y. Fujii, K. Satake, S. Sakai, M. Shinohara, and T. Kanazawa (2011), Joint inversion of strong motion, teleseismic, geodetic, and tsunami datasets for the rupture process of the 2011 Tohoku earthquake, *Geophys. Res. Lett.*, 38, L00G21, doi:10.1029/2011GL050098.
- Zhu, L. and D. Helmberger (1996). Advancement in source estimation technique using broadband regional seismograms., *Bull. Seism. Soc. Am.* 86, 1634-1641

Author affiliation

Bertrand Delouis:

Géoazur, Université de Nice Sophia Antipolis, Observatoire de la Côte d'Azur, CNRS, 250 rue Albert Einstein, 06560 Valbonne delouis@geoazur.unice.fr

Tables

Table 1. Earthquake data.

Name	Date YYYY/MM/ DD	Lat (°N)	Long (°E)	Depth (km)	Mw	Ref	Source of data
ChiChi	1999/09/20	23.85	120.82	8	7.6	GCMT; Chang et al. (2000); Ji et al. (2003); Ma et al. (2001)	CWB
Tottori	2000/10/06	35.27	133.35	12	6.7	GCMT; Ohmi et al. (2002); Iwata and Sekiguchi (2002); Semmane et al. (2005)	K-NET
Aquila	2009/04/06	42.35	13.38	9	6.3	GCMT; Cirella et al. (2009)	ITACA-NET, INGV
Chengkung	2003/12/10	23.11	121.32	18	6.8	GCMT; CWB; Wu et al. (2006)	CWB
Lesser Antilles (Saintes, France)	2004/11/21	15.76	-61.50	10	6.3	GCMT; Feuillet et al. (2011)	RAP
Tarapaca	2005/06/13	-20.01	-69.64	108	7.8	Delouis and Legrand (2007)	RAGIC
Tocopilla	2007/11/14	-22.33	-70.16	45	7.7	GCMT; Delouis et al. (2009b)	RAGIC
Miyagi-Oki	2005/08/16	38.15	142.28	42	7.2	GCMT; JMA and K-NET	K-NET
Tokashi-Oki	2003/09/25	41.78	144.08	17	8.0	JMA and K- NET; Yagi (2004)	K-NET
Tohoku-Oki	2011/03/11	38.19	142.68	21	8.9 to 9.1	Chu et al. (2011)	K-NET
Near Lourdes French Pyrenees	2006/11/17	43.03	0.0	10	4.5	Sylvander et al. (2008); IGN	RAP

Lat: latitude; Long: longitude; Ref: references for the hypocentral location and moment magnitude Mw. For all acronyms, see Data and Resources Section.

Table 2. Fixed source parameters.

	Initial M_{wi}	Half duration of triangular elementary functions (s)	Total available rupture length (km)	Number of point sources	Spacing of point sources (km)
Chichi	7.6	2.3	171	9	19
Tottori	6.7	1.2	50	5	10
Aquila	6.2	0.8	25	5	5
Chengkung	6.7	1.2	50	5	10
Saintes	6.4	0.9	30	5	6
Tarapaca	7.8	2.7	225	9	25
Tocopilla	7.7	2.5	198	9	22
Miyagi-Oki	7.2	1.7	98	7	14
Tokashi-Oki	8.0	3.2	297	9	33
Tohoku-Oki	9.0	6.8	1179	9	131
Near Lourdes	4.5	0.2	1.3	1	1.3

Total available rupture length is twice that given by empirical relations (Wells and Coppersmith, 1994), and is centered on the hypocenter.

Table 3. Results of the FMNEAR inversions.

	Similarity with reference FM	Mw (comp / ref)	Rupture length km (comp / ref)	Dominant directivity (comp / ref)	Actual fault plane selected	First secondary solution close to AUX or REAL and its RMS difference with best solution	Conf. Index	Norm. RMS misfit	Num. of comp retained / initial	Remark concerning the FM solution found with FMNEAR
Chichi	Excellent	7.5 / 7.6	114 / 82	N / N	yes	AUX 0.06	88%	0.31	30 / 48 = 63%	
Tottori	Very good	6.6 / 6.7	20 / 24	SSE / SSE	yes	AUX 0.14	86%	0.33	33 / 57 = 58%	
Aquila	Excellent	6.2 / 6.3	20 / 26	SE / SE	no	REAL 0.04	85%	0.27	27 / 54 = 50%	
Chengkung	Good	6.8 / 6.8	40 / 34	N / S	no	REAL 0.06	56%	0.42	20 / 45 = 44%	
Saintes	Fair	6.2 / 6.3	24 / 20	(-) / (-)	(yes)	AUX 0.04	89%	0.26	10 / 15 = 67%	More strike-slip
Tarapaca	Fair	7.6 / 7.8	75 / 36	(SW) / N	(yes)	AUX 0.1	80%	0.44	12 / 18 = 67%	Fault strike rotated 40°, dip overestimated by 15-25°
Tocopilla	Excellent	7.5 / 7.7	176 / 165	S / S	yes	AUX 0.15	89%	0.20	10 / 18 = 56%	
Miyagi-Oki	Barely Fair	7.0 / 7.1 to 7.2	84 / 57	(NE)/(-)	(yes)	AUX 0.06	77%	0.33	19 / 39 = 49%	Fault strike rotated 30 to 40°, dip overestimated by 25-30°, more strike-slip
Tokashi-Oki	Barely fair	7.9 / 8.0	231 / 130	W / SW	(yes)	AUX 0.01	62%	0.40	12 / 42 = 29%	Fault strike rotated 20 to 40°, dip overestimated by 25 to 35°.
Tohoku-Oki	Fair	8.7 / 8.9 to 9.1	393 / 360	S / (-)	no	REAL 0.06	87%	0.44	13 / 36 = 36%	Fault dip overestimated by 35-45°
Near Lourdes	Excellent	4.55/4.4	-----	-----	-----	-----	92%	0.41	19 / 33 = 58%	

Similarity with reference FM: qualify the similarity between the Focal Mechanism (FM) computed with FMNEAR with the reference (published) FM solutions. **Mw (comp / ref):** value of the FMNEAR moment magnitude (Mw) / reference (published) value of Mw. **Rupture length km (comp / ref):** value of rupture length computed with FMNEAR / rupture length derived from published slip map. The value from FMNEAR corresponds to the distance

along strike (discretized by point sources) along which seismic moment amounts for at least 20% of the maximum moment release. **Dominant directivity (comp / ref)**: direction of dominant directivity computed from FMNEAR / from reference (published) slip map. “(-)” means no dominant directivity along strike, and “(direction)” means that the difference in seismic moment between the dominant rupture direction and the opposite direction is less than 10%, i.e. that rupture is nearly bilateral. **Actual fault plane selected**: “yes”: the nodal plane selected by FMNEAR corresponds to the known rupture plane. “no”: the nodal plane selected by FMNEAR is the auxiliary plane of the actual rupture plane. “(yes)” when there are nonetheless noticeable differences in strike, dip, or rake. **First secondary solution close to AUX or REAL and its RMS difference with best solution**: AUX or REAL corresponds to the first secondary solution close to the auxiliary plane or to the real plane, depending on whether the best solution corresponds to the real or the auxiliary plane respectively. The value indicated after AUX or REAL is the difference between the RMS misfit function of that solution with the RMS of the best solution. This to quantify the difference in misfit between the actual rupture plane and the auxiliary plane. **Conf. Index**: confidence index (see text). **Norm RMS misfit**: normalized Root Mean Square misfit function for the best solution. Variance reduction in percentage is $(1-\text{RMS}) \times 100$. **Num. of comp retained / initial**: number of components (N, E, or Z) finally retained / number of components initially included in the inversion, and corresponding ratio value in percent

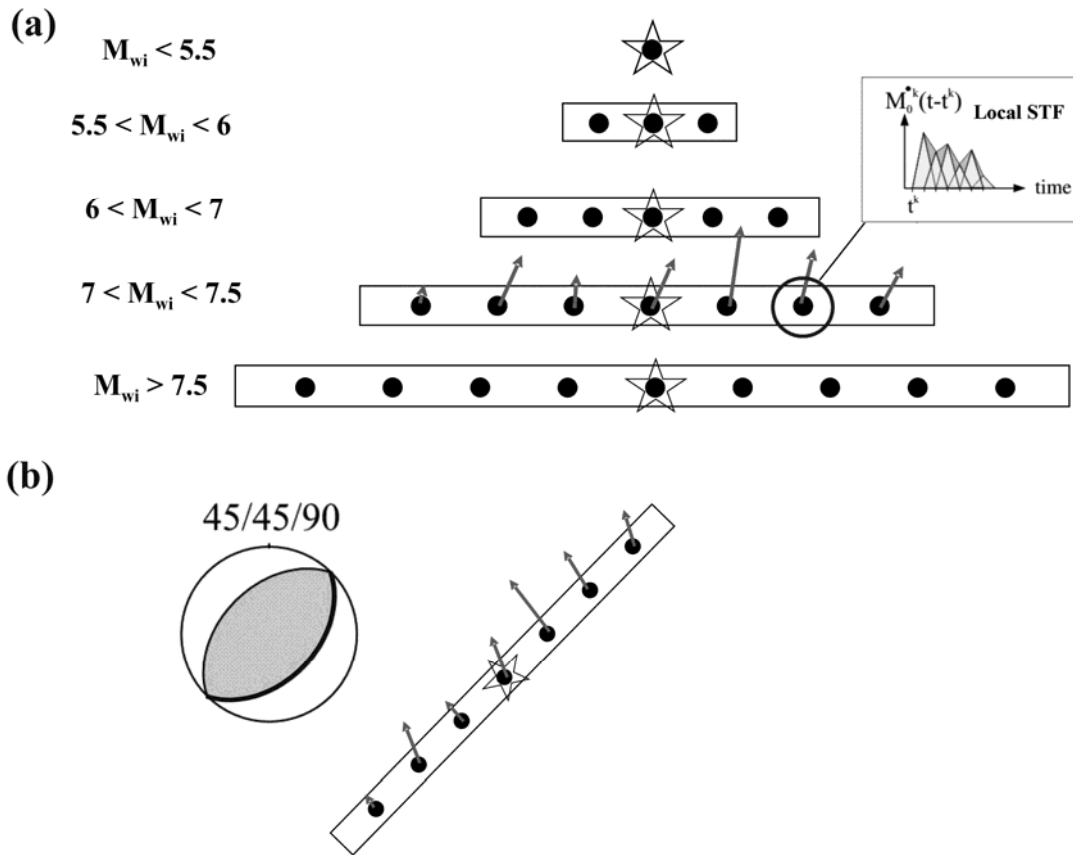


Figure 1. Source model used in the FMNEAR method. (a) For magnitude larger than 5.5 (M_{wi} , a priori magnitude) a finite dimension line source model is used, based on an uneven number (3, 5, 7, or 9) of point sources (black dots) depending on the magnitude range. The star in the middle position is the hypocenter. For smaller events ($M_{wi} < 5.5$) a simple point source model is used. For illustration, the relative variation of seismic moment and the variability of rake are displayed for the case $7 < M_{wi} < 7.5$. with the arrows (arbitrary scale). Also shown, for one of the point sources (number k), the local source time function (STF) corresponding to the local moment rate function. The dot above M_0 indicates the time derivative; t_k is the rupture onset time of the point source k . (b) Example of orientation of the line source model for tested focal mechanism corresponding to strike/dip/rake = 45/45/90. The star is located at the hypocenter and the line is oriented along the strike.

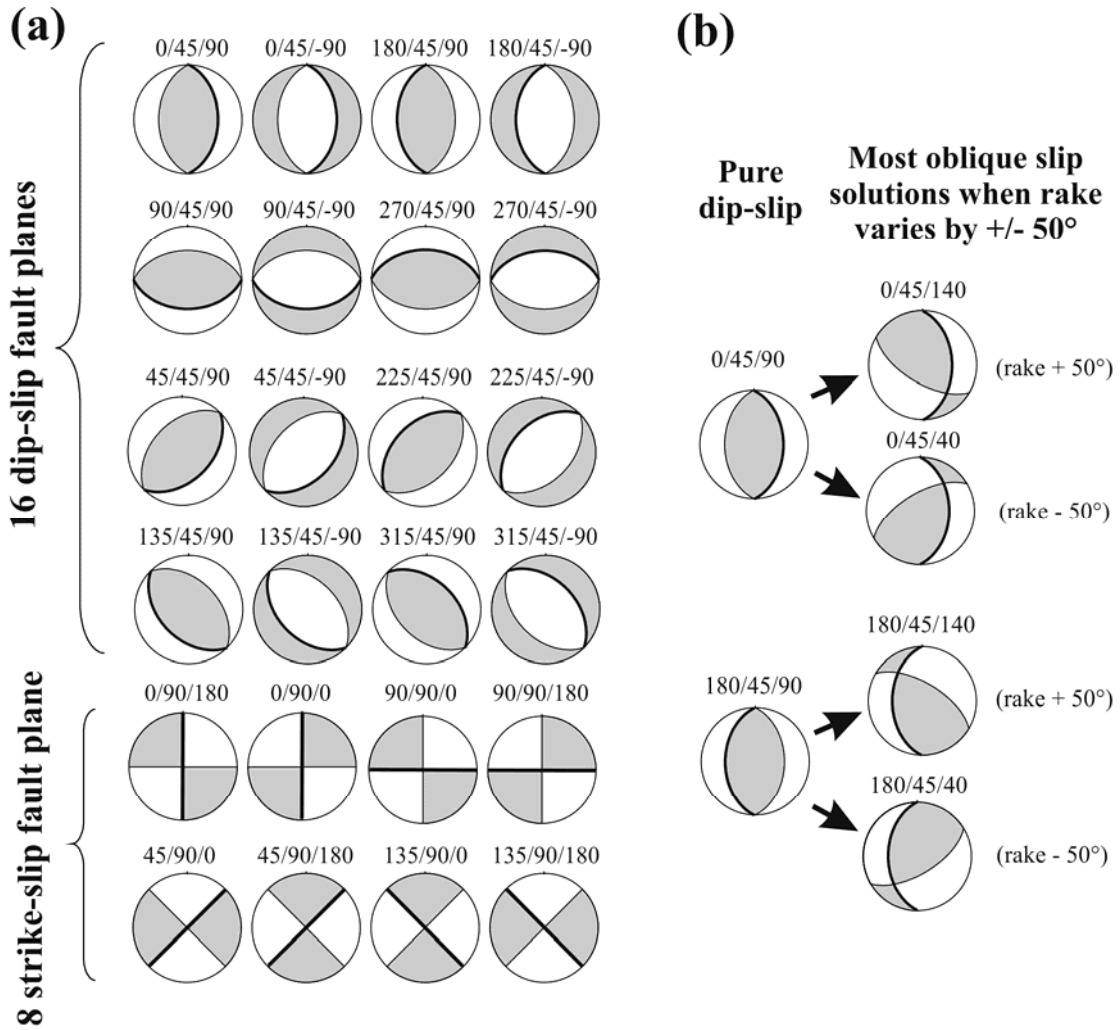


Figure 2. (a) The 24 fault planes (16 dip-slip and 8 strike-slip) tested in step 1 of the grid search of the focal mechanism. The numbers above each beach ball indicate the strike/dip/rake values. The rake indicated here is a central value, the rake inverted by simulated annealing being allowed to vary around that value with a maximum deviation of $\pm 50^\circ$. (b) Illustration of the variable obliquity in the focal mechanisms explored when the rake is inverted with a possible deviation of $\pm 50^\circ$ around the central value. Two fault planes, in pure dip-slip in this example, corresponding to the same focal mechanism, give rise to different oblique faulting mechanisms. In (a) and (b), and in the following Figures, focal mechanisms are represented in the lower hemisphere projection. The fault plane is drawn with a heavy black line.

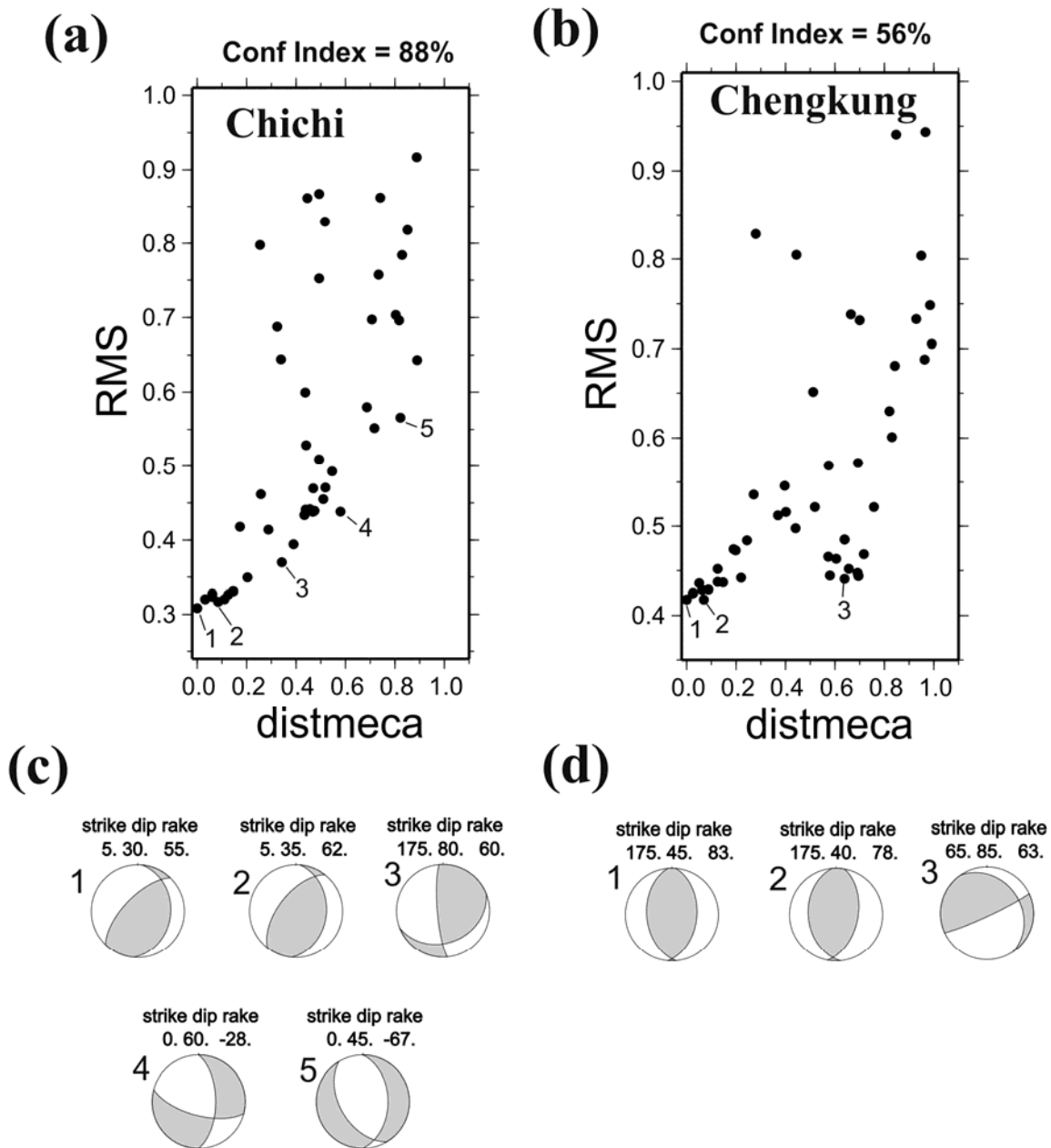


Figure 3. Illustration of the solutions explored in the cases of the Chichi (left, a and c) and Chengkung (right, b and d) earthquakes. The two plots at the top (a and b) show the explored solutions (black dots) in graphs RMS waveform misfit versus distance between focal mechanisms (FM). Some chosen solutions are labeled with numbers, and focal mechanisms corresponding to these solutions are drawn at the bottom (c and d). Distance here is computed between the solution considered and the best solution (number 1). In the Chichi case, solutions exhibit RMS values increasing rapidly as a function of distance. Consequently the confidence index is high (88%). In the case of Chengkung, the group around solution labeled “3” has FM very different from the best FM solution although their RMS values are only slightly higher than the best solution. Consequently the confidence index is low (56%).

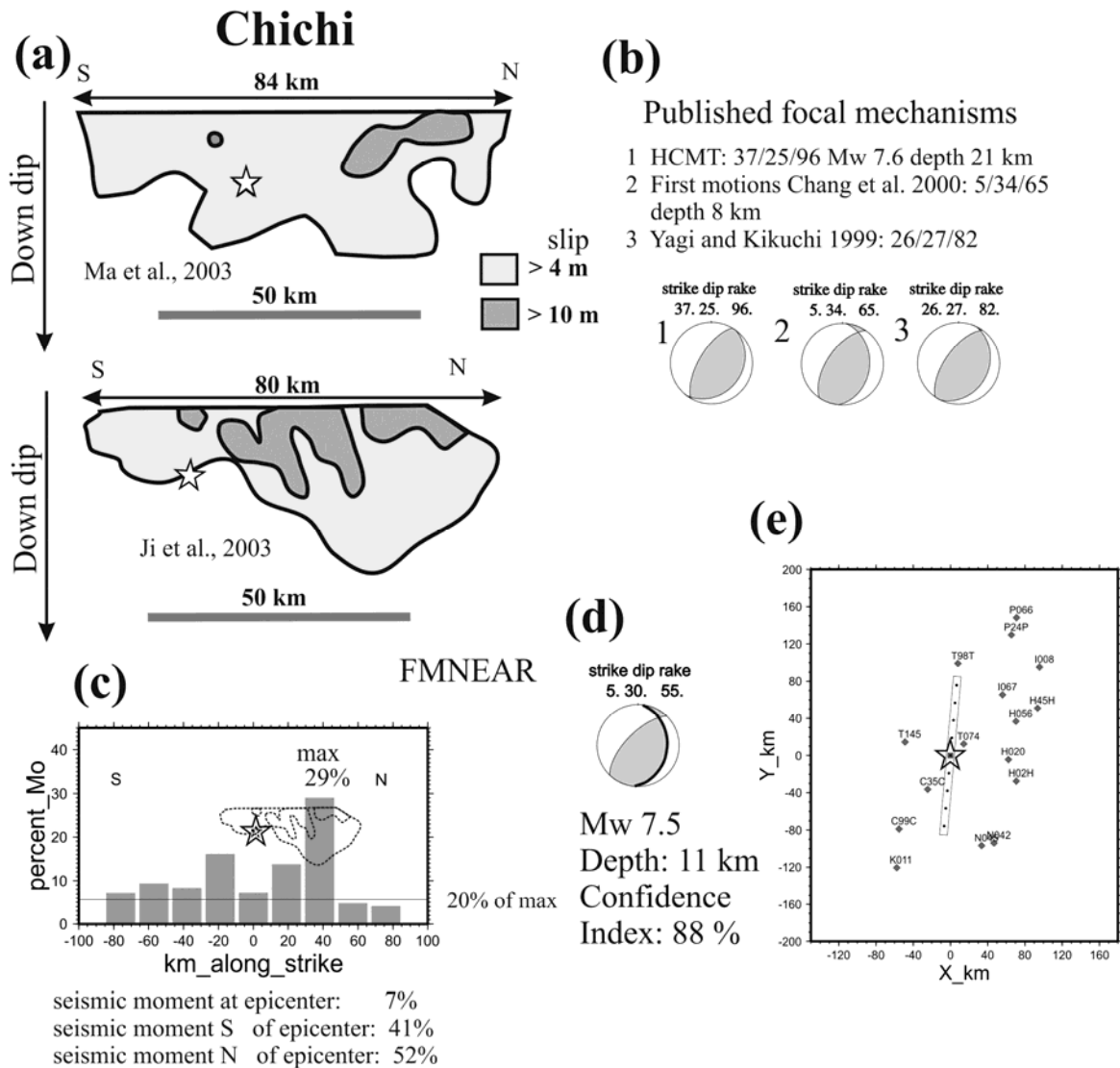


Figure 4. Results for the Chichi earthquake. Top left (a): published slip distributions redrawn in a simplified way, with two thresholds in slip values, 20% (light gray) and 50% (darker gray) of maximum slip. Star: hypocenter. Slip distributions from Ma et al. (2003) and Ji et al. (2003). Top right (b): published focal mechanisms for the event, with the corresponding references. Bottom left (c): histogram distribution of the percentage of total seismic moment (M_0) along strike found by FMNEAR. The orientation of the line source model is given; the star indicates the position of the epicenter. The maximum percentage of seismic moment is indicated (max). The thin horizontal line is used as a threshold to measure rupture length. It corresponds to 20% of the maximum of moment release. Below the histogram, the percentages of seismic moment at the epicenter and in the two opposite directions along fault strike are presented. The slip map (here that of Ji et al., 2003) is drawn at the same scale on the histogram for an easy comparison. Bottom center (d): best solution found by FMNEAR for the focal mechanism, together with the indication of the final moment magnitude (M_w), selected depth, and confidence index. Selected nodal plane with thick black line. Bottom right (e): map with the strong motion stations used (diamonds), the surface projection of the line source model (rectangular frame with point sources represented by black dots), and the epicenter (star). X axis towards the East, Y axis towards the North

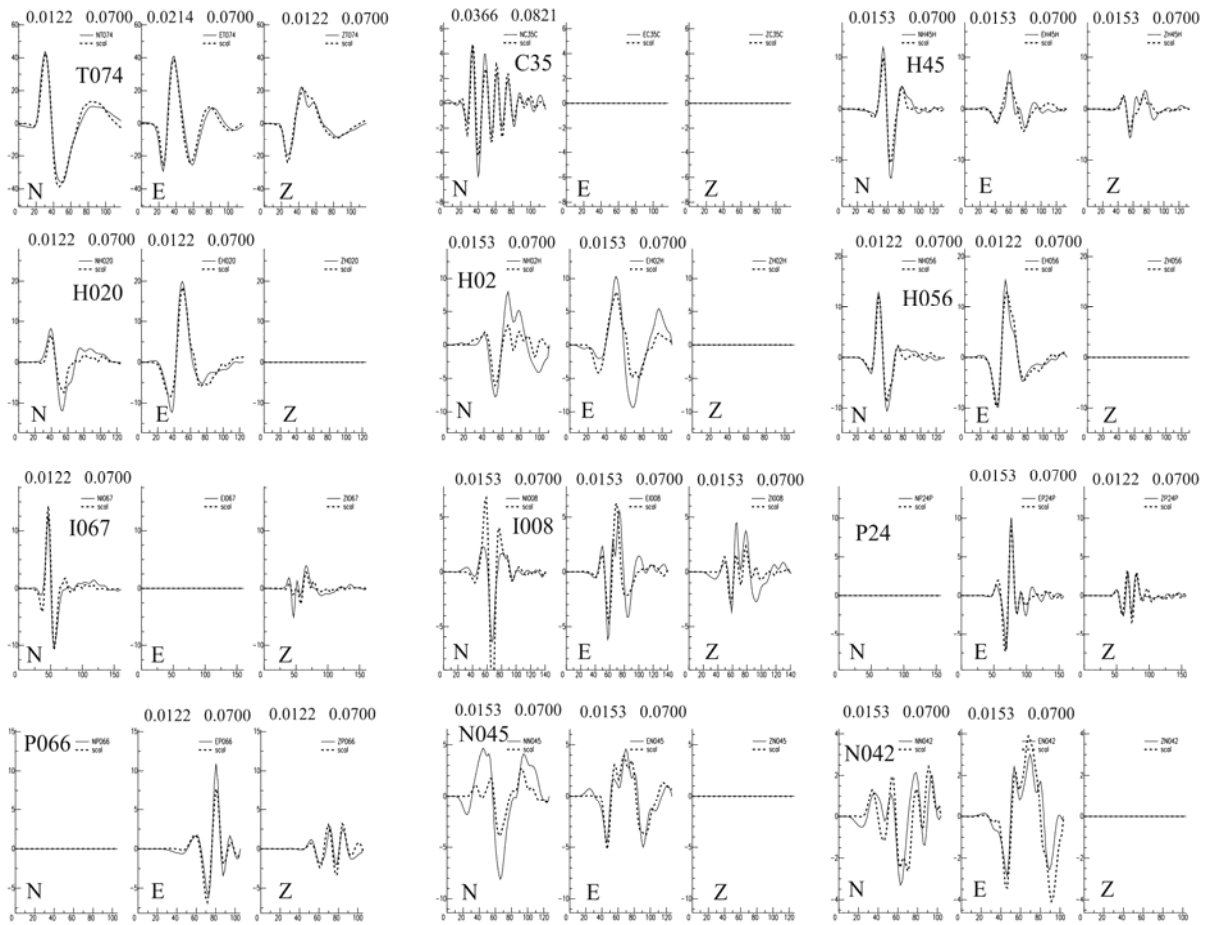


Figure 5. Waveform modeling for the Chichi earthquake. Horizontal axis, time in seconds. Vertical axis, displacement amplitude in centimeters. Continuous line: observed; dashed line: computed. Numbers above signals indicate the frequency band in Hz (filtering between f_{min} and f_{max} , see text). Components where the observed and computed signals are flat correspond to components which were discarded by the inversion.

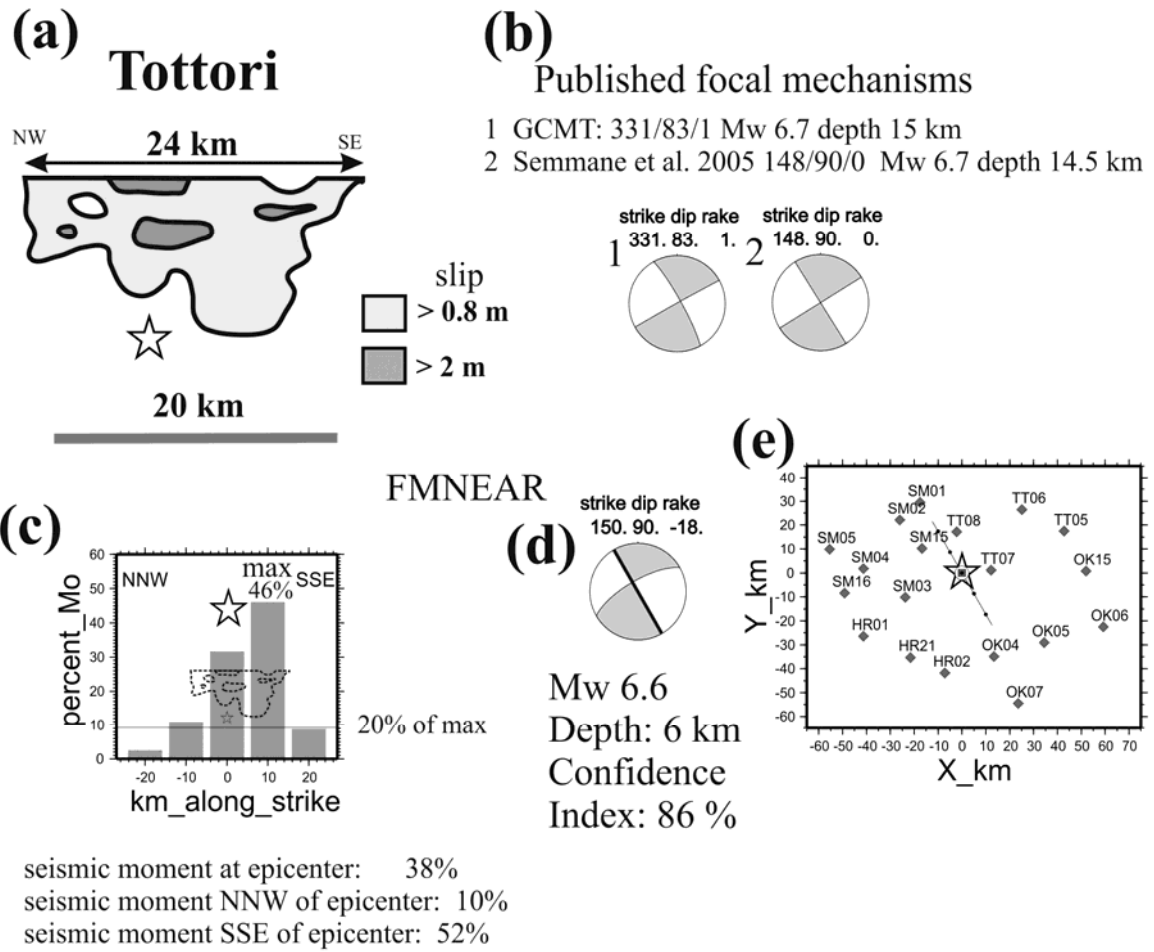


Figure 6. Results for the Tottori earthquake. Same caption as Figure 4, but slip distribution from Semmane et al. (2005)

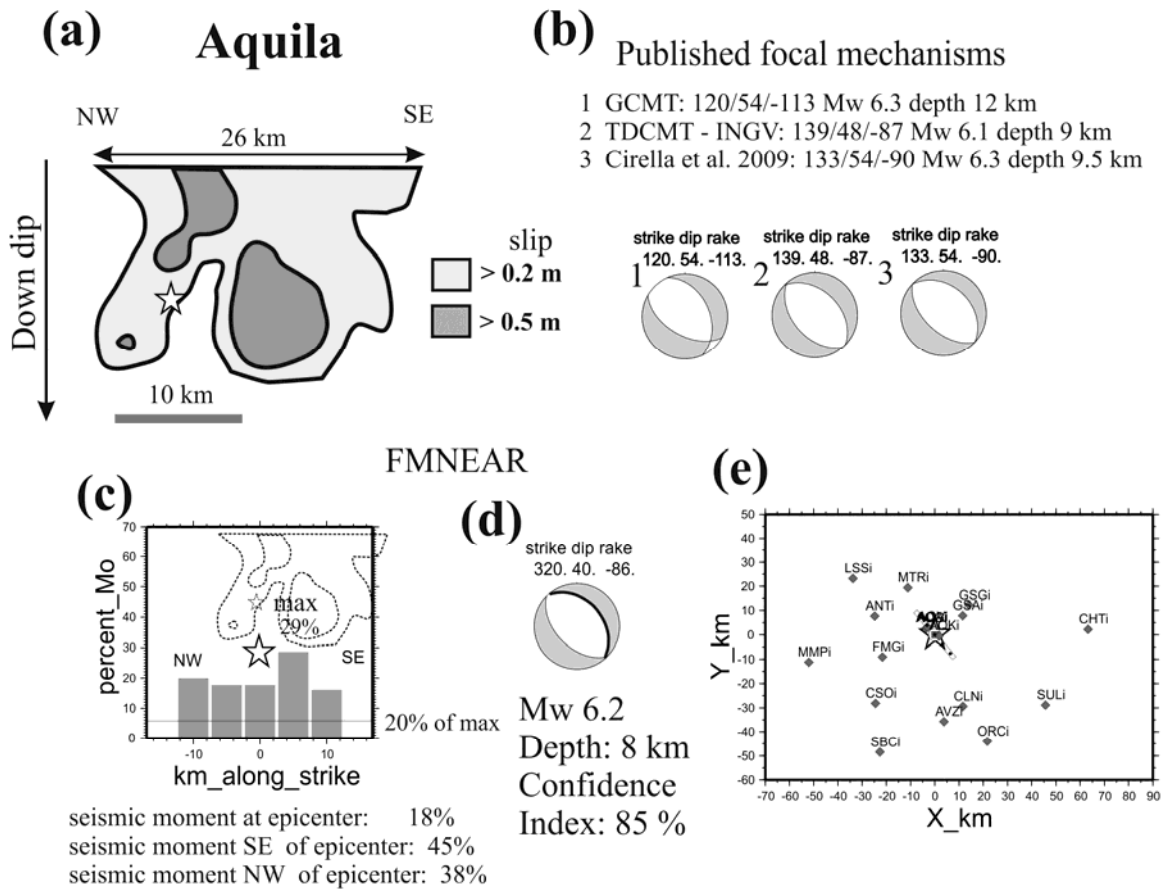


Figure 7. Results for the Aquila earthquake. Same caption as Figure 4, but slip distribution from Cirella et al. (2009).

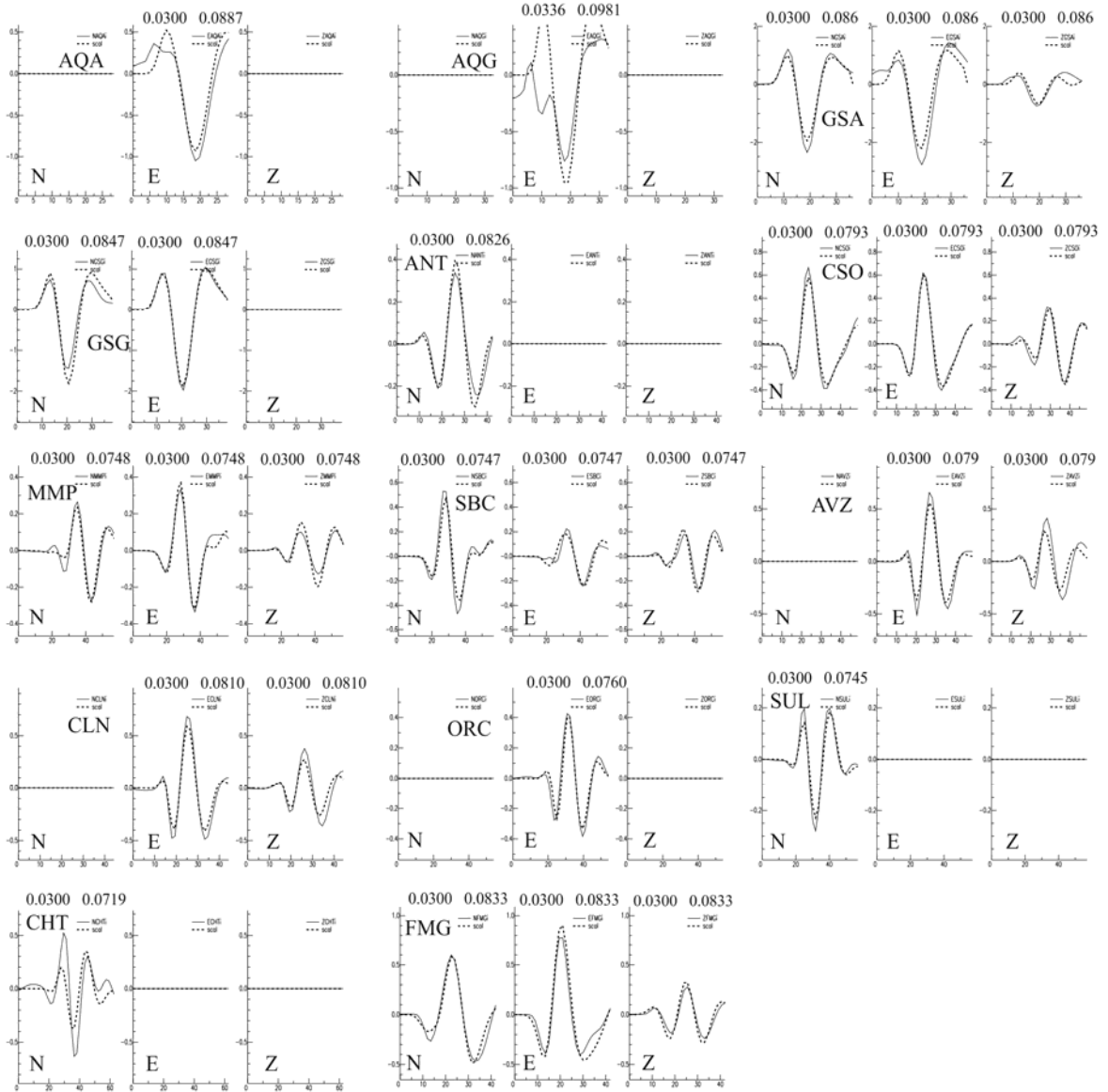


Figure 8. Waveform modeling for the L'Aquila earthquake. Same caption as Figure 5.

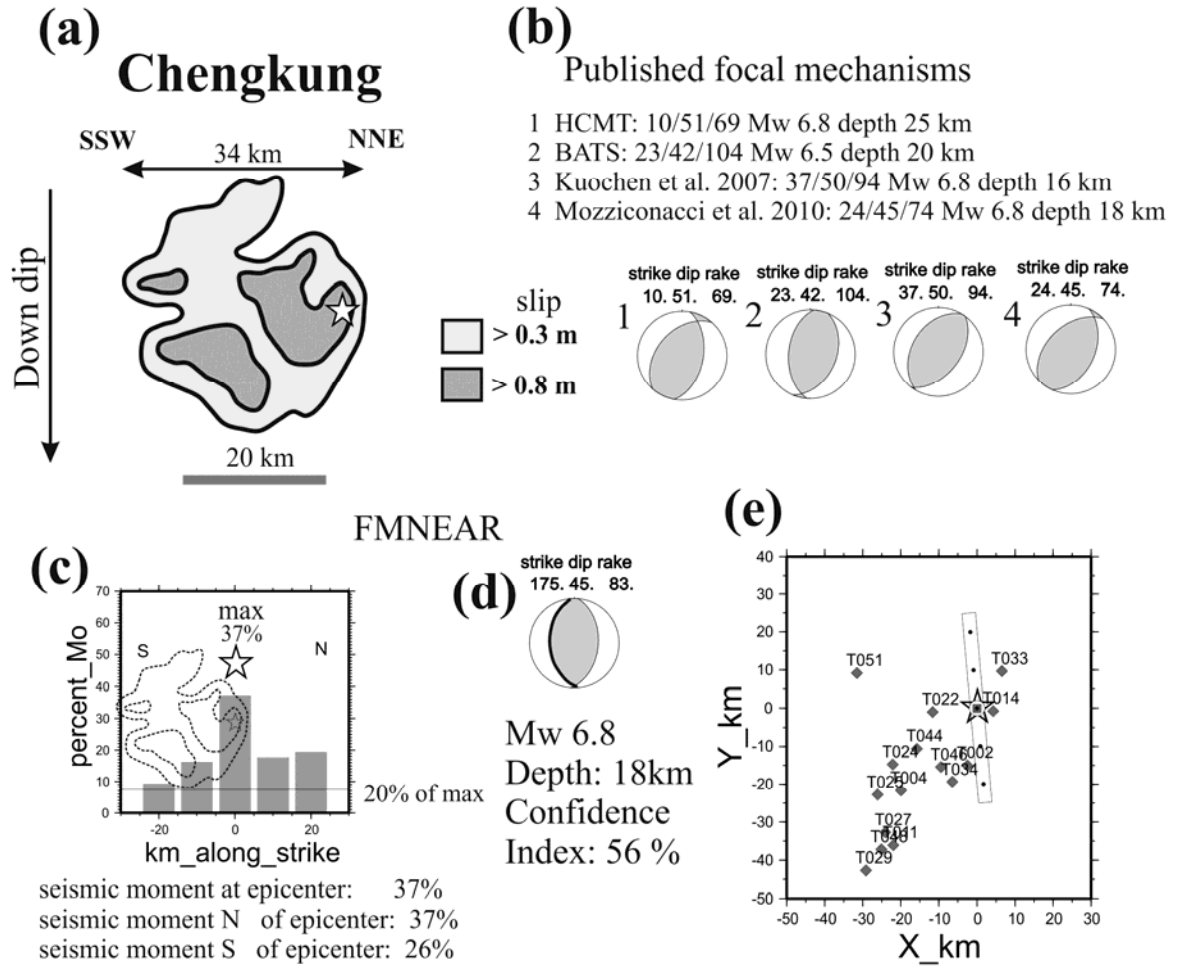


Figure 9. Results for the Chengkung earthquake. Same caption as Figure 4, but slip distribution from Mozziconacci et al. (2009).

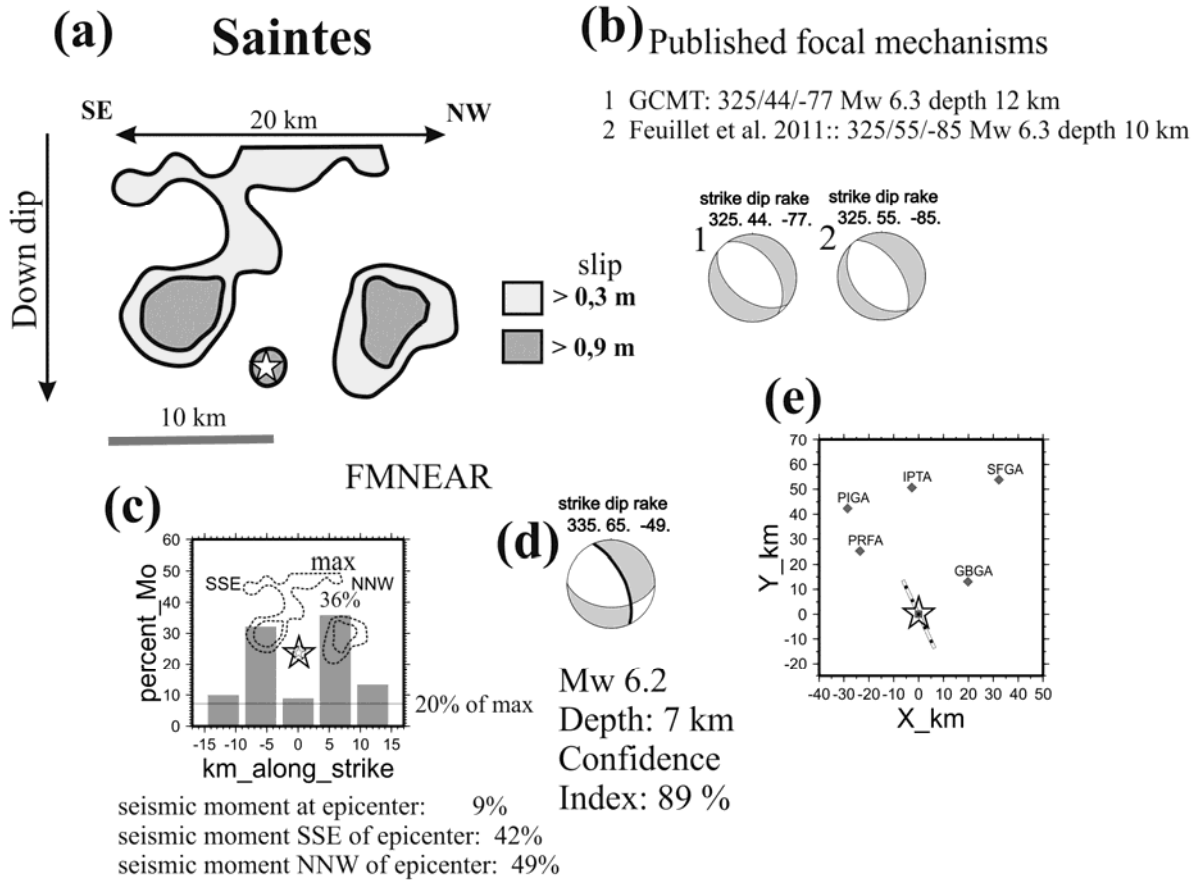


Figure 10. Results for the Saintes earthquake. Same caption as Figure 4, but slip distribution from Feuillet et al. (2011).

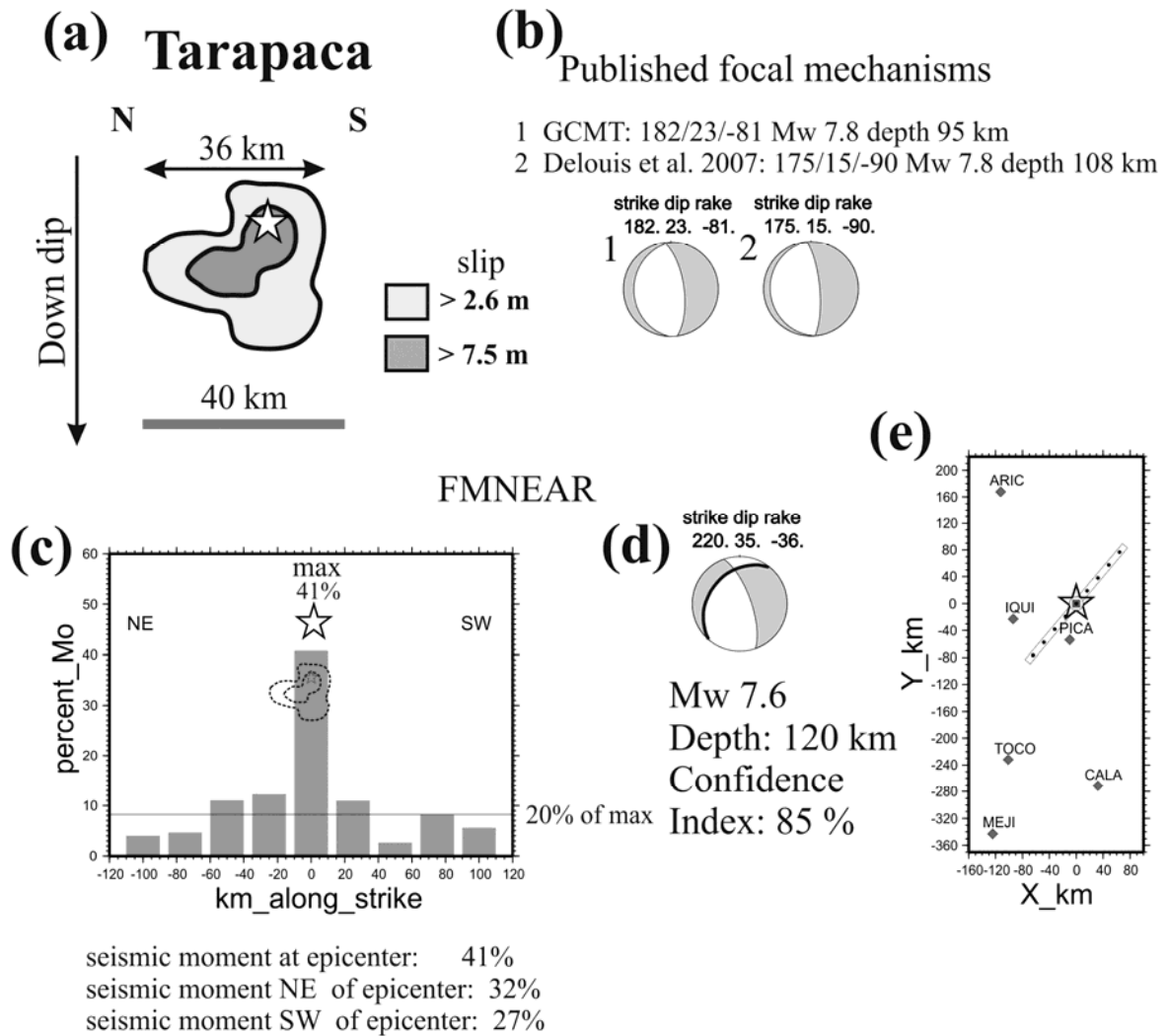


Figure 11. Results for the Tarapaca earthquake. Same caption as Figure 4, but slip distribution from Delouis and Legrand (2007).

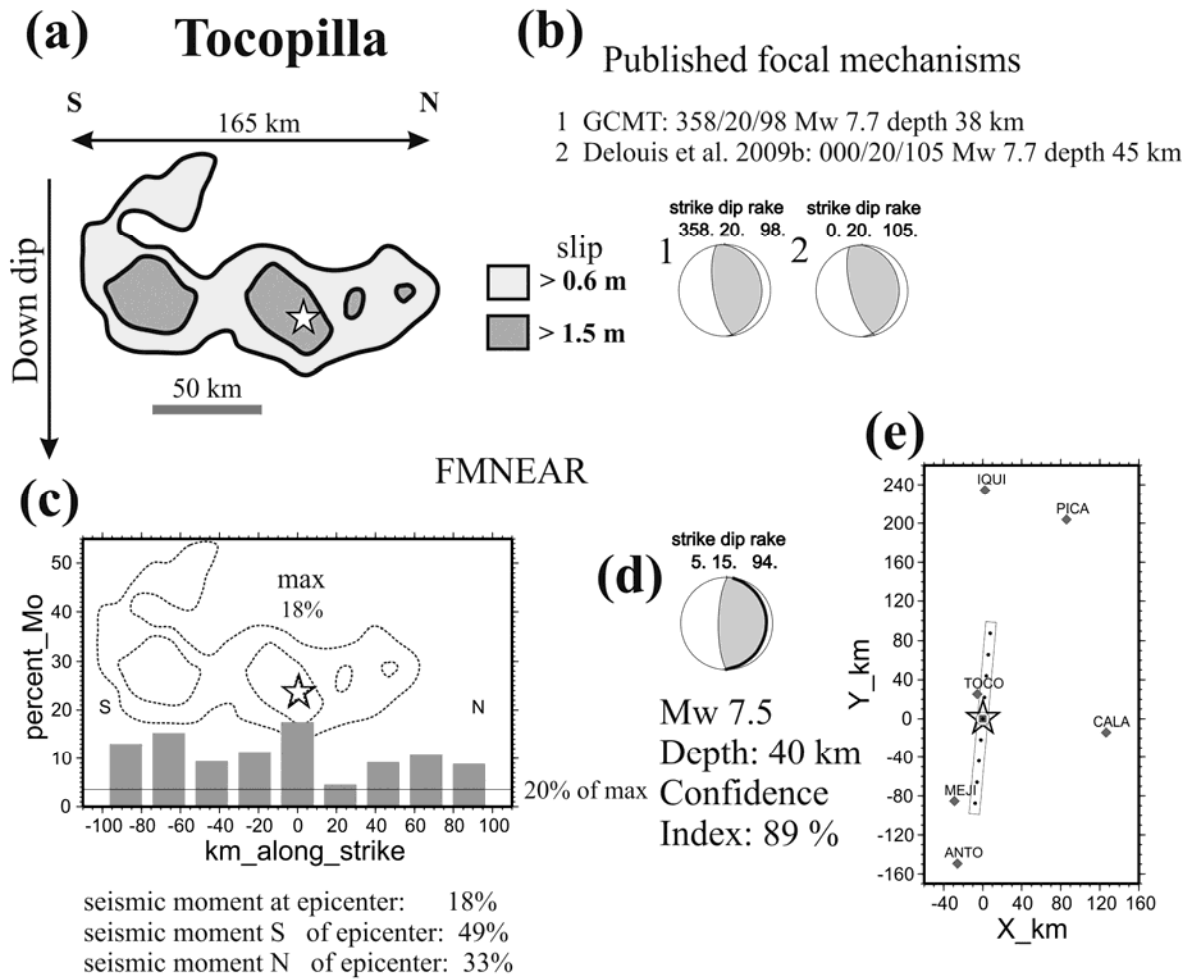


Figure 12. Results for the Tocopilla earthquake. Same caption as Figure 4, but slip distribution from Delouis et al. (2009b).

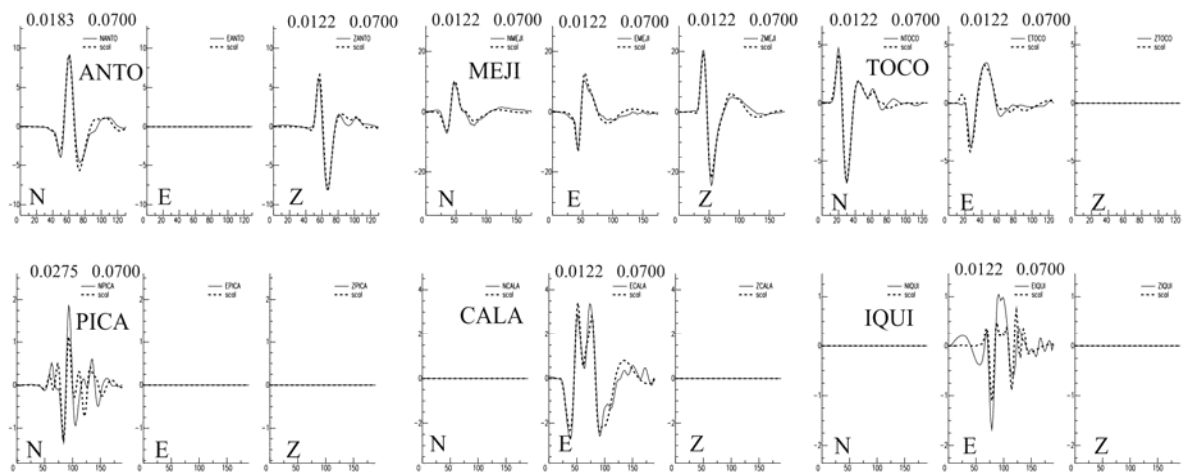


Figure 13. Waveform modeling for the Tocopilla earthquake. Same caption as Figure 5.

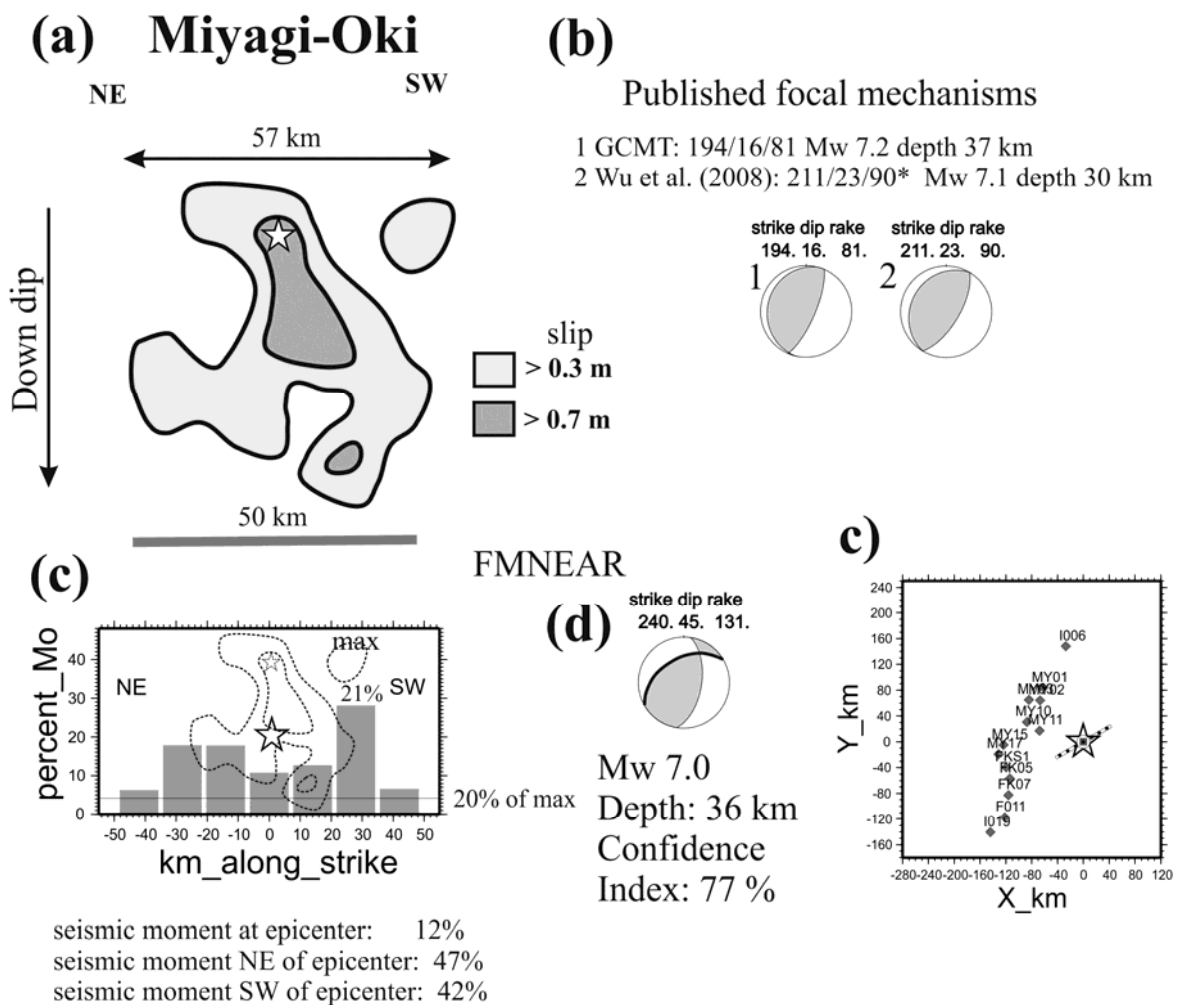


Figure 14. Results for the Miyagi-Oki earthquake. Same caption as Figure 4, but slip distribution from Wu et al. (2008).

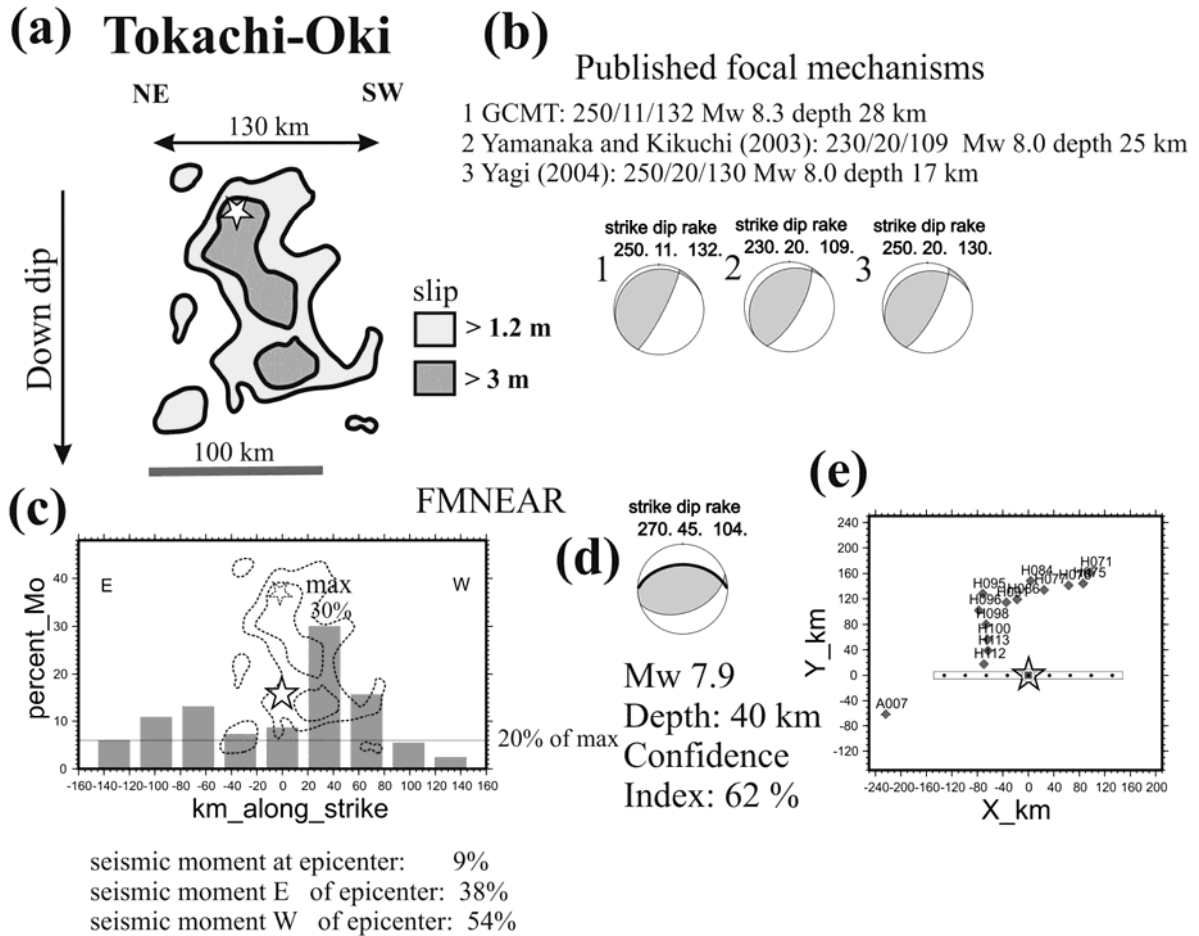


Figure 15. Results for the Tokachi-Oki earthquake. Same caption as Figure 4, but slip distribution from Yagi (2004).

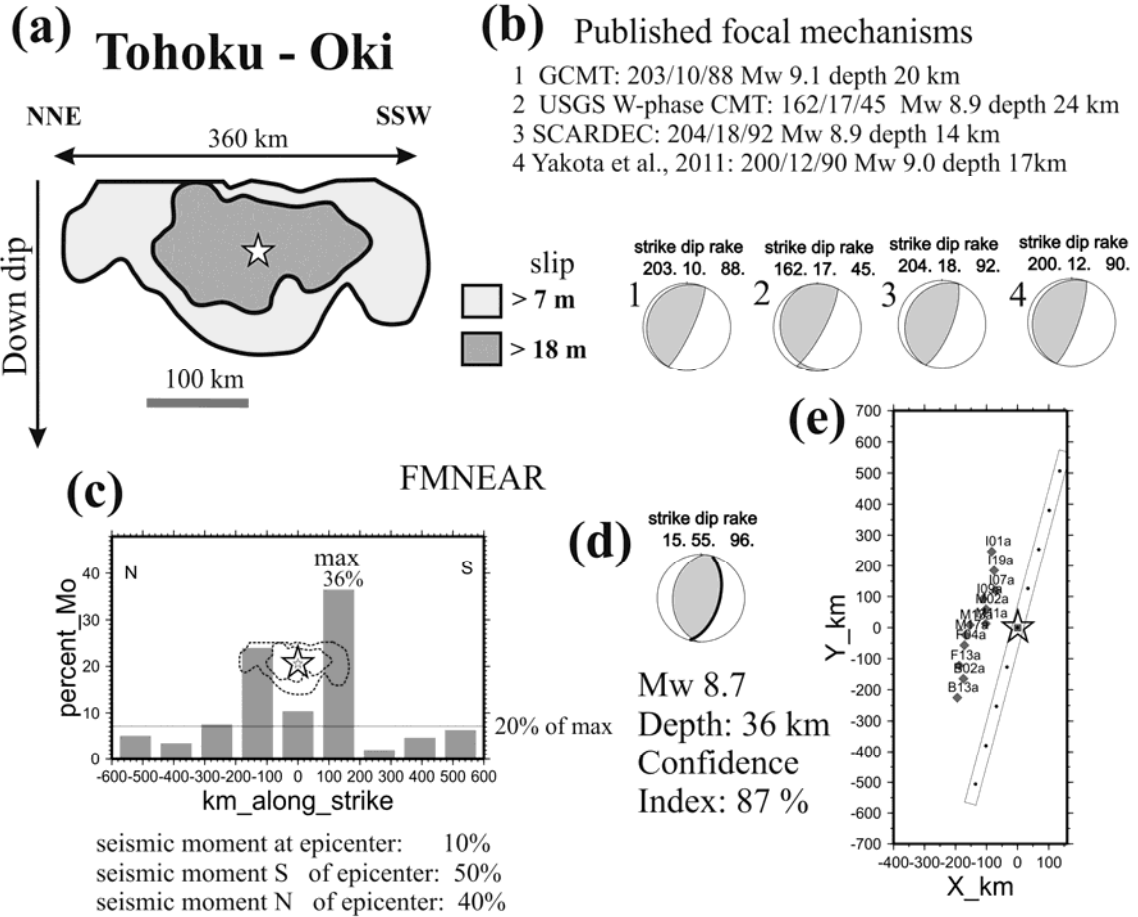


Figure 16. Results for the Tohoku-Oki earthquake. Same caption as Figure 4, but slip distribution from Yakota et al. (2011).

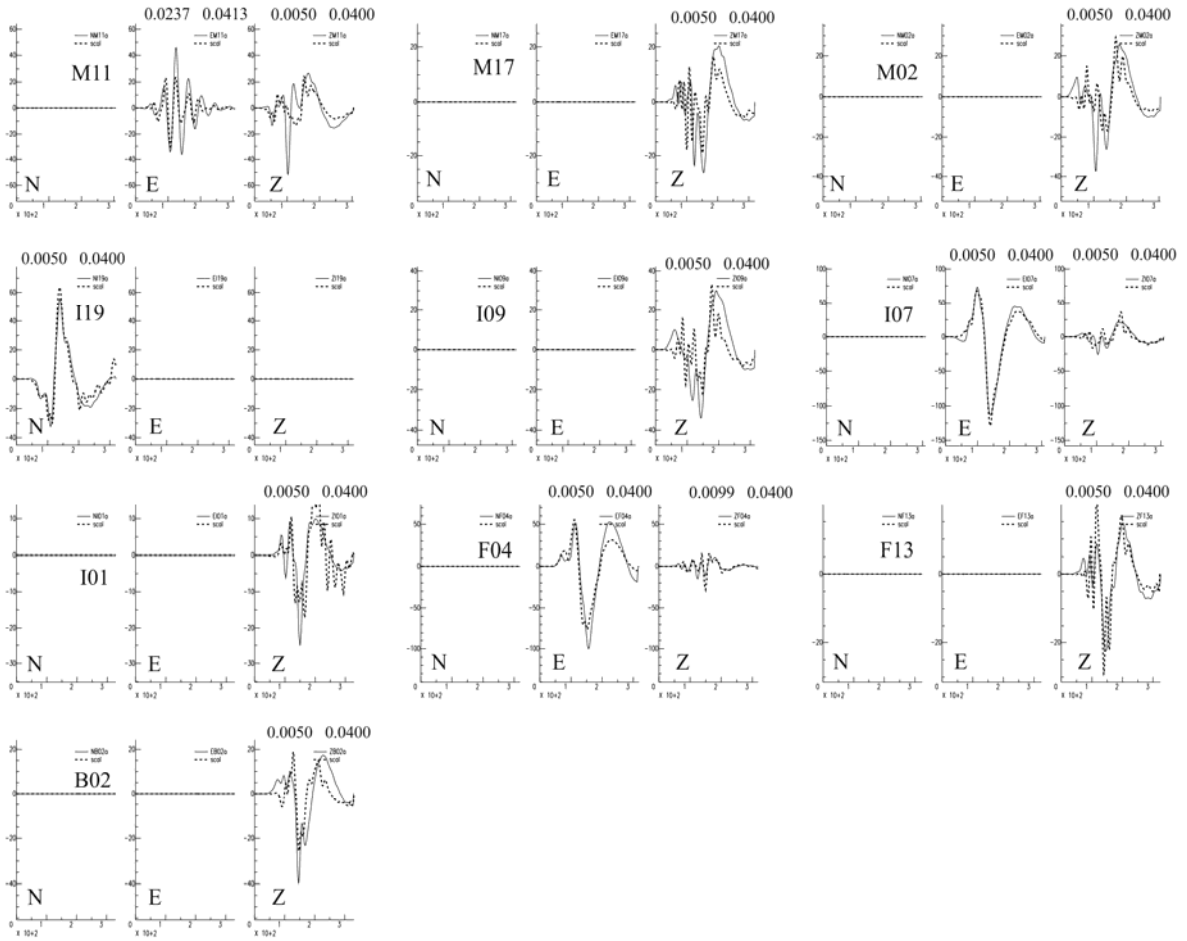


Figure 17. Waveform modeling for the Tohoku-Oki earthquake. Same caption as Figure 5.

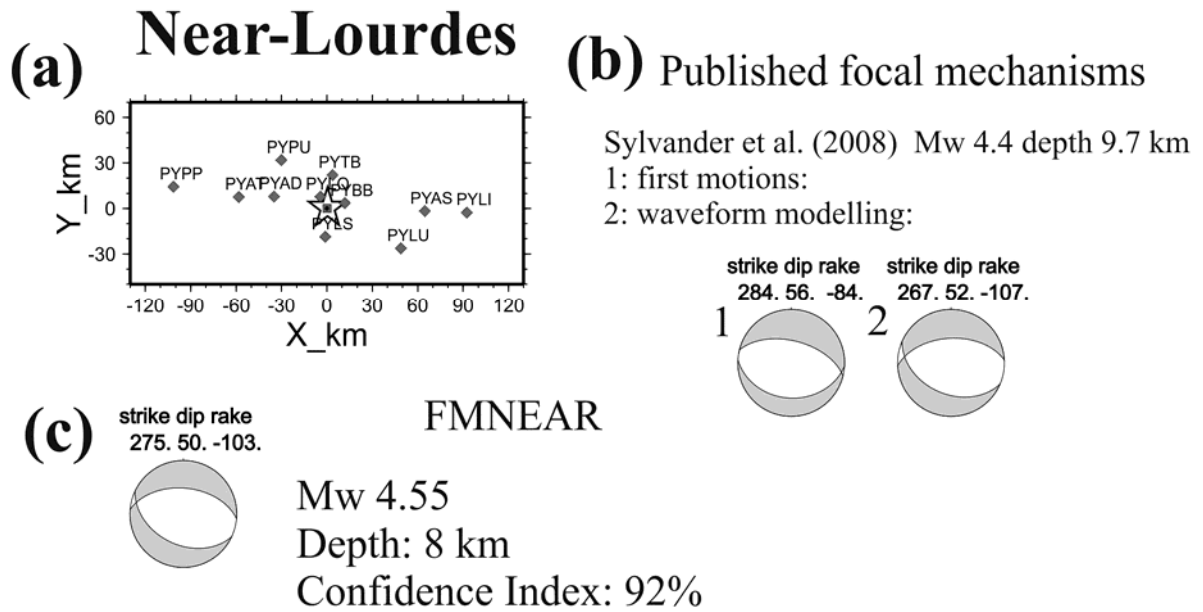


Figure 18. Results for the moderate size Near-Lourdes earthquake. The source here is a single point source. Top left (a): map with the strong motion stations used (diamonds) and the epicenter (star). X axis towards the East, Y axis towards the North. Top right (b): published focal mechanisms for the event, with the corresponding reference. Bottom left (c): best solution found by FMNEAR for the focal mechanism, together with the indication of the final moment magnitude (M_w), selected depth, and confidence index.

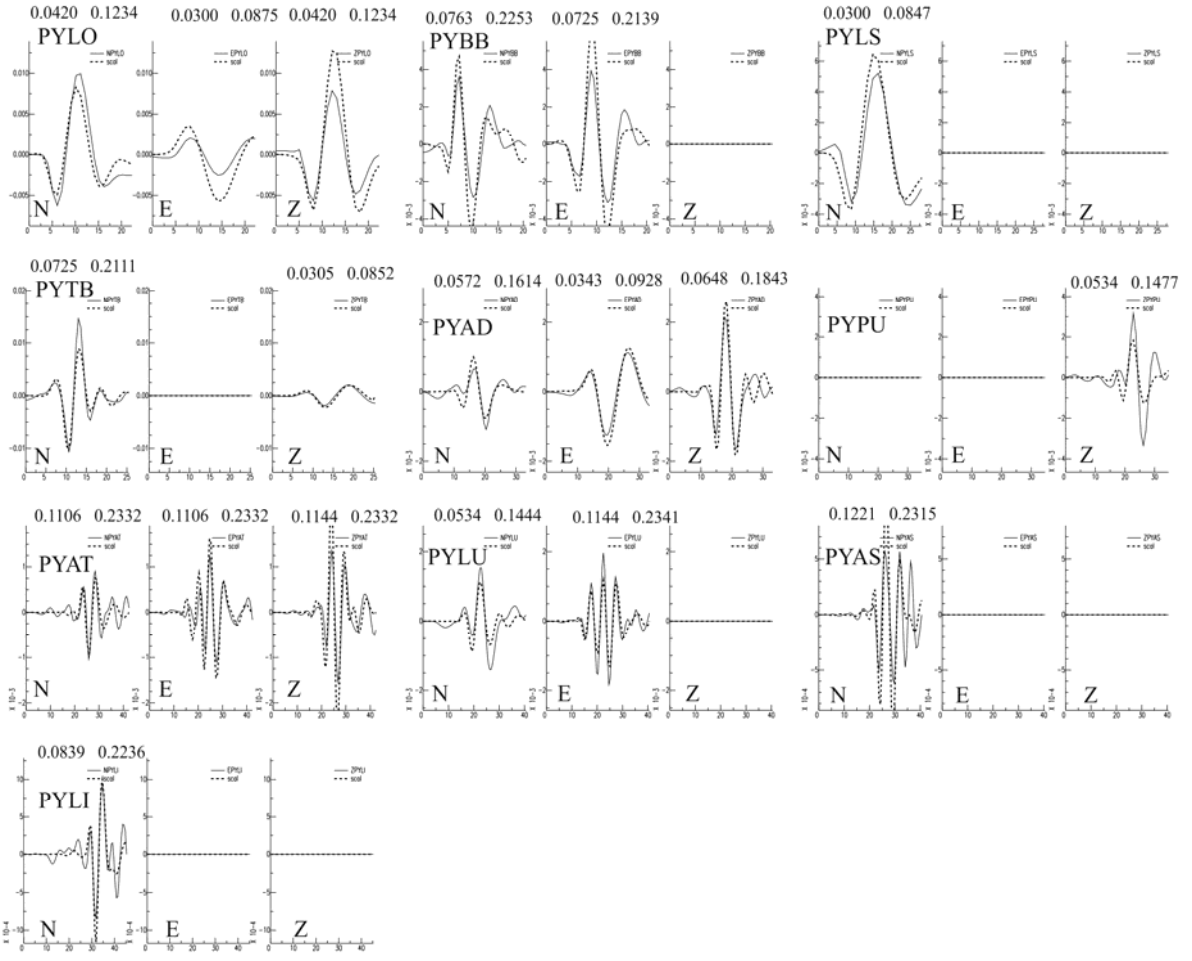


Figure 19. Waveform modeling for the Near-Lourdes earthquake. Same caption as Figure 5.

Electronic supplement to

FMNEAR: determination of focal mechanism and first estimate of rupture directivity using near source records and a linear distribution of point sources

by Bertrand Delouis

The Electronic supplement presents the explicit formulation of several parameters used in the FMNEAR inversion: maximum frequency, upper bound of the bandpass filtering, length of the time window used in the inversion, width of the triangular individual time windows used to discretize the local source time functions, minimization of the seismic moment, depth exploration, and computation of the index of confidence. It also contains complementary Figures detailing some aspects of the FMNEAR method, such as flow charts (Figures S1 and S2), computation of the distance between focal mechanisms (Figure S3), waveform fit for 6 earthquakes among the test cases considered in the paper (Figures S4 to S9), the results of sensitivity tests discussed in the paper (Figures S10 and S12), and the waveform fit for an inversion of the Chichi earthquake where individual components were not discarded on the basis of waveform fit (Figure S11). Finally, Table S1 describes the crustal velocity models used with the test cases.

Computation of maximum frequency (called here f_{max} , the upper bound for the bandpass filtering) as a function of initial magnitude (M_{wi}) and hypocentral distance (dist)

f_{max} is basically fixed to 3 f_{min} (the lower bound for the bandpass filtering), but we apply some additional conditions:

If $M_{wi} > 6$: f_{max} cannot be higher than $0.1 + (6 - M_{wi})/300$

If M_{wi} in the range 4 to 6: f_{max} cannot be higher than $0.2 + (5 - M_{wi})/10$

If $M_{wi} < 4$: f_{max} cannot be higher than $1.5 + (2 - M_{wi})/1.67$

Then we apply a correction as a function of hypocentral distance:

$f_{max} = f_{max} - (dist/3500)$ where dist is in km

Finally we impose some minimum value for f_{max} , which is 0.04 Hz for very large earthquakes ($M_{wi} > 8.5$) and 0.07 Hz otherwise.

Length of the time window used in the inversion

First we estimate a minimum duration (dur_{min}) as a function of the propagation time of the S wave (t_{calS}) and the rupture length (L) estimated from Wells and Coppersmith (1994):

$dur_{min} = t_{calS} + L/1.5$ (in seconds)

where 1.5 represents a slow rupture velocity in km/s.

Then, we use different empirical formulas to obtain the final length of the time window:

If $M_{wi} < 4$, final length = durmin + (dhypo/10) + 1.3/fmin + 4 (in seconds)

If $M_{wi} > 4$, final length = 1.3 durmin + (dhypo/8) + 0.35/fmin + 5 (in seconds)

Where M_{wi} is the initial magnitude.

The values of the coefficients in these formulas were progressively adjusted during the analysis of tens of earthquakes spanning a wide range of magnitudes.

Half width of the triangular individual time windows used to discretize the local source time functions

This half width is $10^{(M_{wi} - 6.5)/3}$ (in seconds)

Where M_{wi} is the initial magnitude.

Minimization of the seismic moment

The minimization function which is included in the total cost function of the simulated annealing algorithm, in addition to the RMS misfit function, is the following:

$0.01 \text{ EXP}(M_0/M_{0ref}) - 1$ where M_{0ref} is the reference seismic moment obtained from the initial magnitude M_{wi} , M_0 the seismic moment of the current solution explored, and EXP the exponential function.

Depth exploration

Primary 7 depths tested (in addition to initial depth):

If initial depth < 20 km: 2, 5, 10, 20, 30, 40, 50, 70 km (wide range of exploration since routine automatic locations often end up with a shallow depth, sometimes fixed)

If initial depth in the range 20 to 45km: 12, 20, 28, 36, 44, 52, 60 km

If initial depth in the range 45 to 75km: 30, 40, 50, 60, 70, 80, 90 km

If initial depth in the range 75 to 150km: 60, 80, 100, 120, 140, 160, 180 km

If initial depth in the range > 150 km: 110, 150, 190, 230, 270, 310, 350 km

If the initial depth gave a better result, it is kept.

For the refined search, 4 additional depths are tested, with a step of 1 km if depth < 15km, a step of 2 km if depth is between 15 and 30 km, and a step of 10 or 20 km for deeper earthquakes.

Computation of the Confidence Index

We have 54 focal mechanism (FM) solutions which have been tested.

Let us consider the best solution, associated with the lowest RMS misfit value (hereafter called "bestrms").

Let us consider one of the 53 other solutions with its RMS value (hereafter called "rms").

For that particular secondary solution, we compute an individual confidence index which is:

$$Ci = 150 [\text{rms}^6 / (\text{bestrms}^{6.2} (1+\text{dist})^4)]$$

Where $dist$ is the distance between the best solution and the secondary solution, as defined in Figure S3 below. The value of 150 and the exponents were empirically adjusted after analysing tens of inversions for different earthquakes over a wide range of magnitudes.

We see that C_i will be small if rms is close to rms_{best} and $dist$ is large. The exponent 6.2 for $best_{rms}$ is to give slightly more weight to the contribution of $best_{rms}$ by itself (when $best_{rms} < 1$, which is generally the case, it will enhance the confidence in case of results displaying small values of $best_{rms}$).

In order to take into account the number of components used in the inversion (a larger number of component meaning a higher confidence), we modify C_i as following:

$$C_i = C_i [ncomp^{0.2} + 0.2]$$

The final confidence index, CI , is the minimum value among all the 53 individual C_i values. As a matter of fact, it is the most penalizing value, corresponding to the lowest C_i value, which has to be taken into account. In other word, $CI = \min (c_i)$.

Remark 1: in order to stabilize individual C_i towards large values, we apply an arc-tangente to it.

Remark 2: we do not allow individual C_i values to be larger than 100.

Remark 3: since CI varies between 0 (lowest confidence) and 100 (highest confidence), we call it a confidence index in %.

Figures

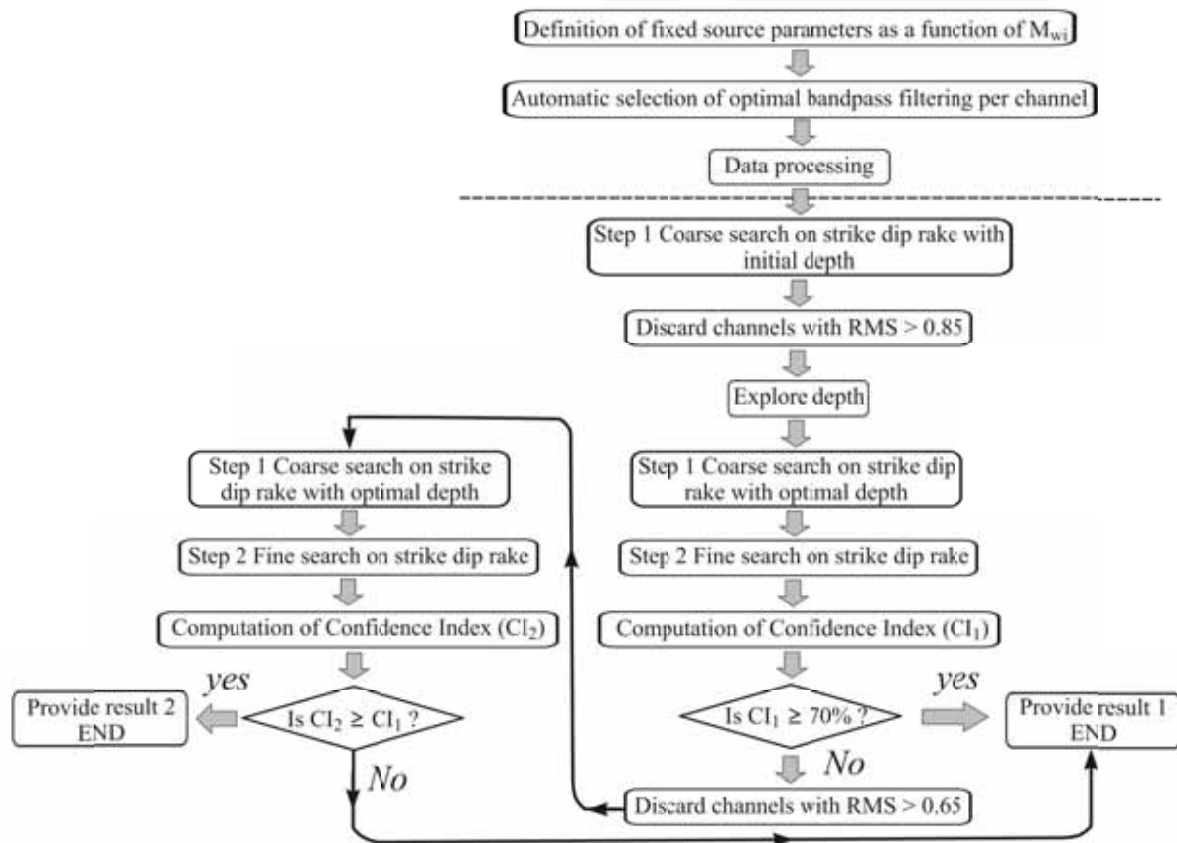


Figure S1. Flow chart of the FMNEAR method. After a complete run of the two steps of the inversion (coarse and fine search on strike dip rake), a confidence index is computed (CI_1). If CI_1 is lower than 70%, the two steps are redone keeping only those channels (components) whose RMS misfit value is smaller than 0.65. A new confidence index (CI_2) is then computed, and the results of this last run are kept only if $CI_2 > CI_1$.

Fine search Step 2

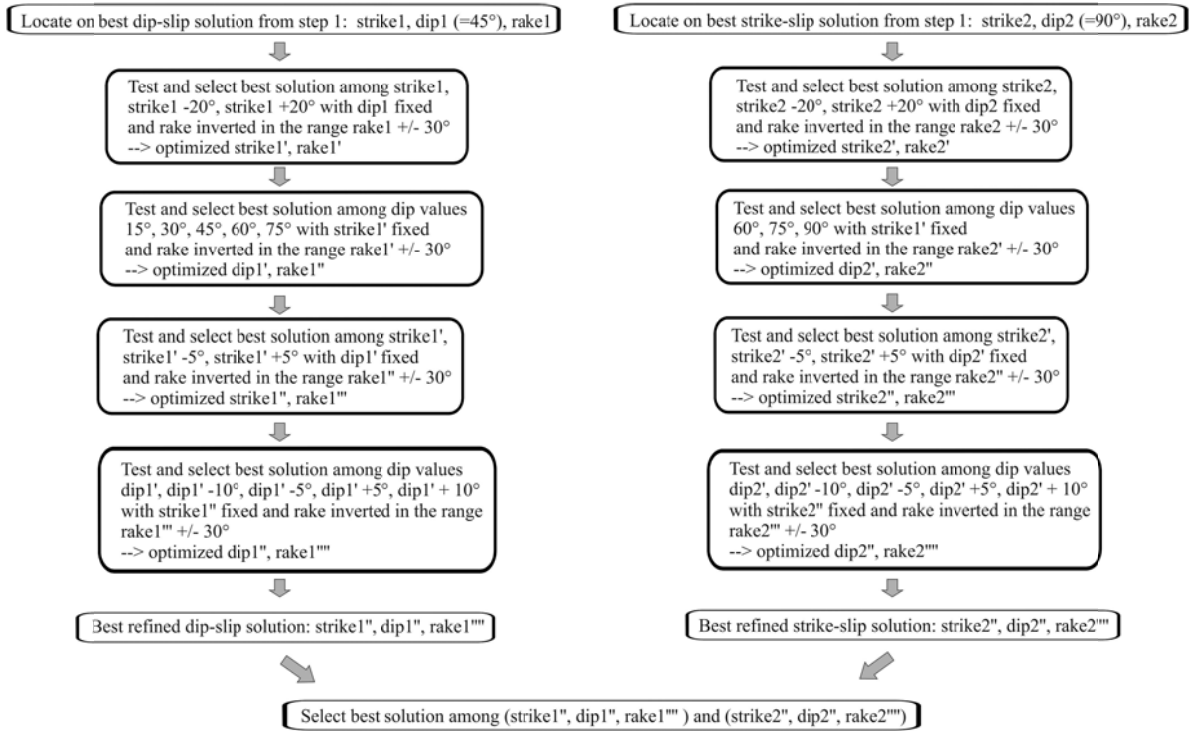
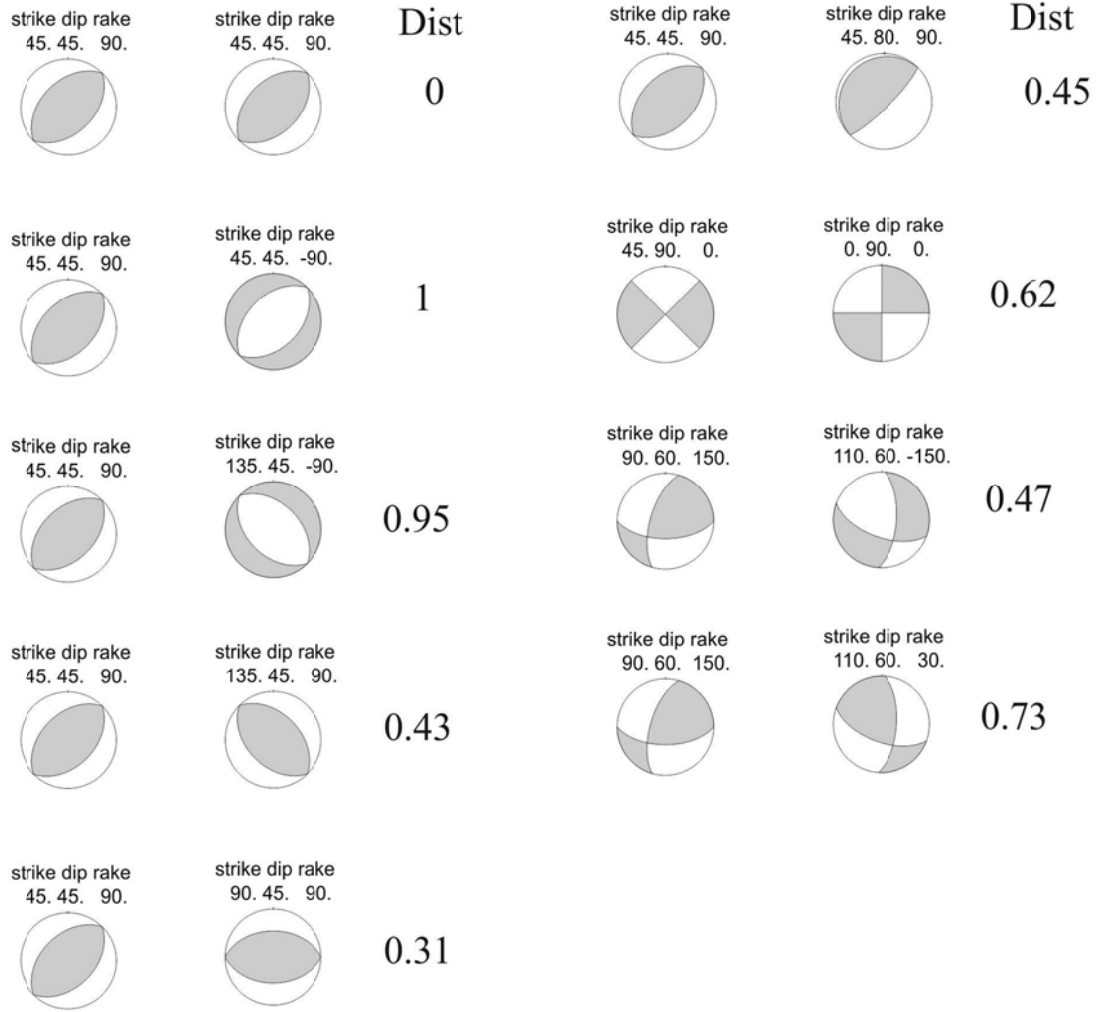


Figure S2. Flow chart detailing step 2 of the FMNEAR method. The left and right columns, corresponding to the exploration around the best dip-slip and best strike-slip solutions respectively, are independent. In each step, the rake angle is inverted jointly with the rupture timing and local source time functions of each point source included in the source model with a simulated annealing algorithm.



$$\text{Distance (FM1 - FM2)} = \frac{1}{m} \sum_{i=1}^m \text{ABS} (\text{amp}_{\text{FM1}} - \text{amp}_{\text{FM2}})$$

$$\text{ampFM} = 2 (\vec{v} \cdot \vec{\gamma}) (\vec{n} \cdot \vec{\gamma})$$

\vec{n} : unit vector normal to the nodal plane

\vec{v} : unit slip vector on the nodal plane

$\vec{\gamma}$: unit vector defining the take-off direction

Figure S3. Illustration of the distance between focal mechanisms (FM). The distance is defined as the sum of the differences, in absolute sense, of the theoretical amplitude of the P wave (ampFM) between the two focal mechanisms, computed over m points sampling the focal sphere. In practice $m=324$. The distance varies between 0 (identical FM) to 1 (opposite FM). The relation giving ampFM, on the Figure, is derived from the radiation pattern of the far field P wave in Aki and Richards (1980).

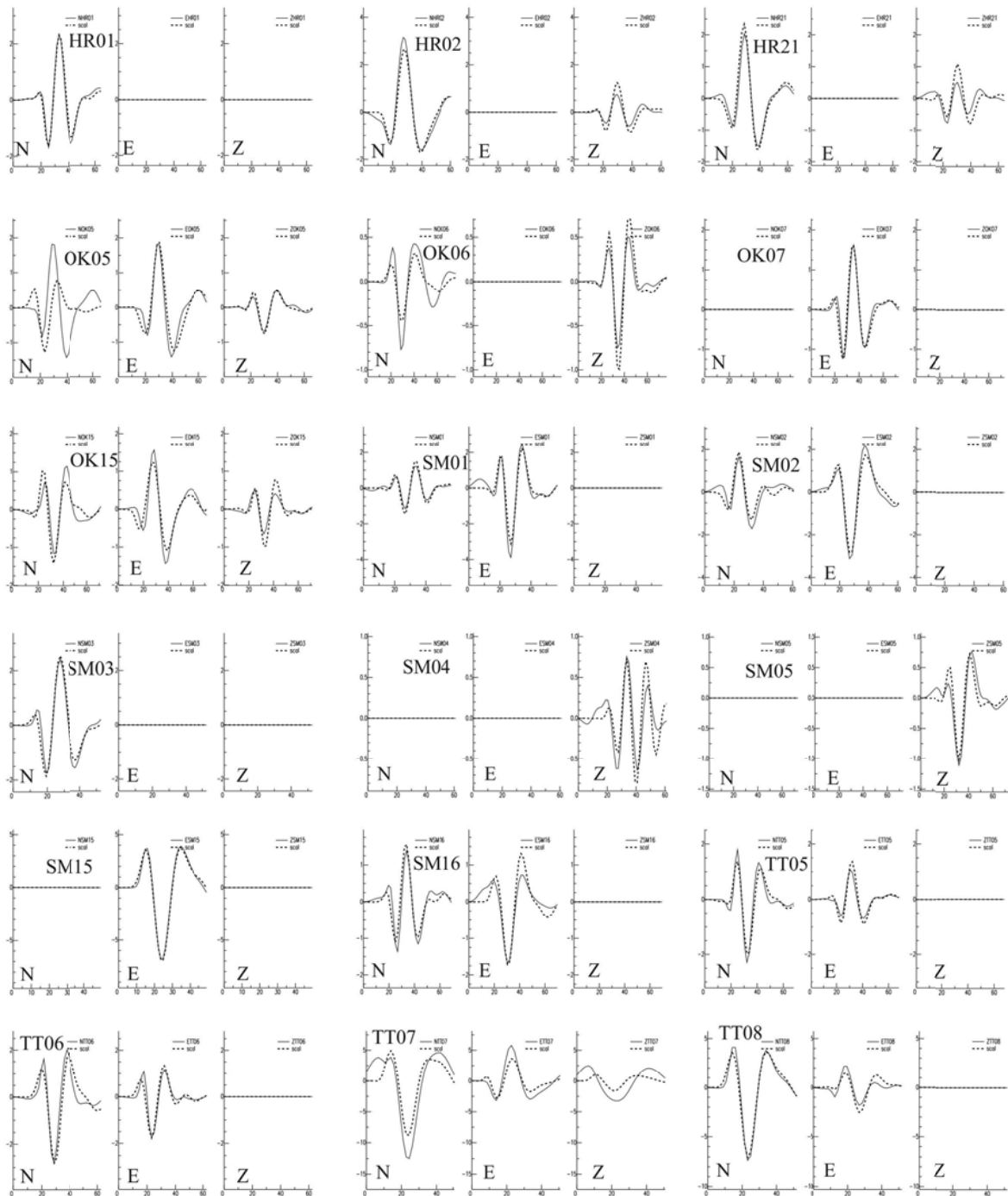


Figure S4. Waveform modeling for the Tottori earthquake. Horizontal axis, time in seconds. Vertical axis, displacement amplitude in centimeters. Continuous line: observed; dashed line: computed. Components where the observed and computed signals are flat correspond to components which were discarded by the inversion.

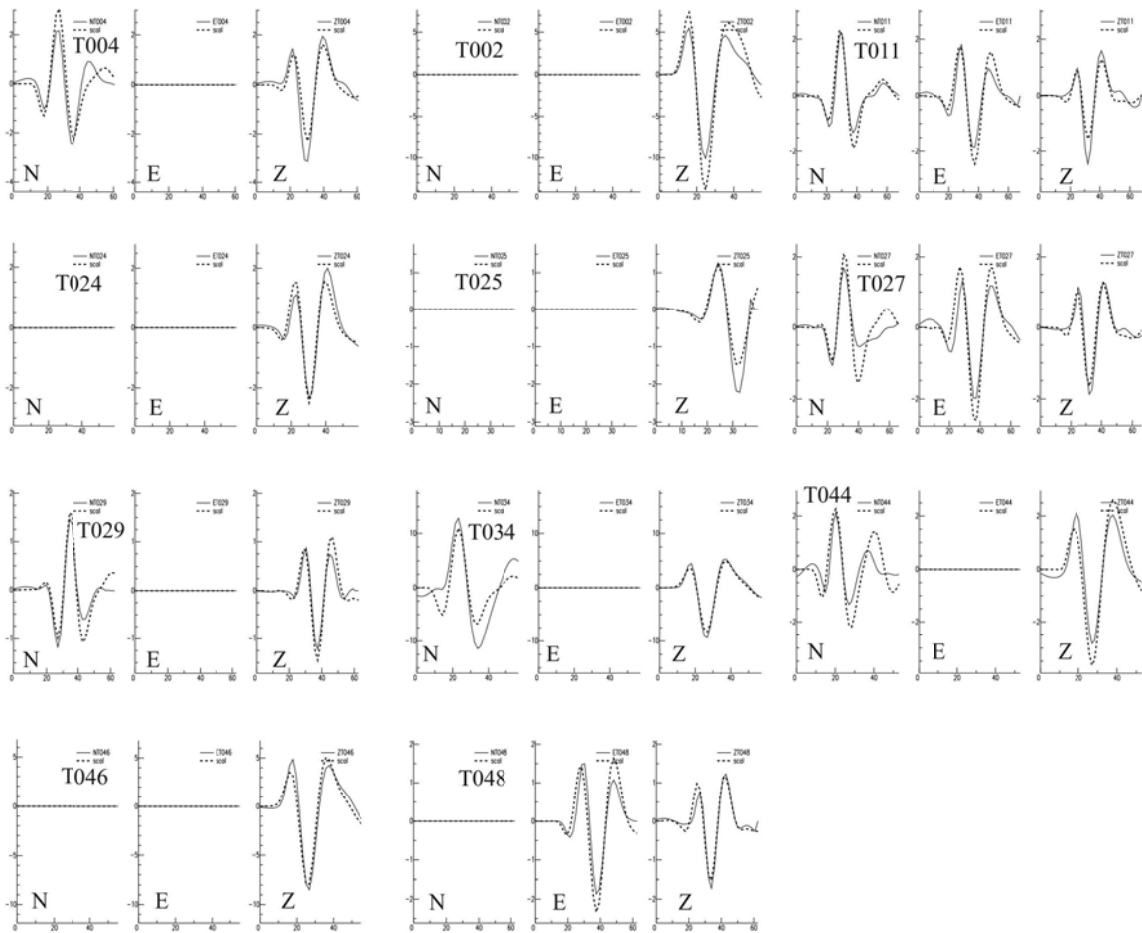


Figure S5. Waveform modeling for the Chengkung earthquake. Horizontal axis, time in seconds. Vertical axis, displacement amplitude in centimeters. Continuous line: observed; dashed line: computed. Components where the observed and computed signals are flat correspond to components which were discarded by the inversion.

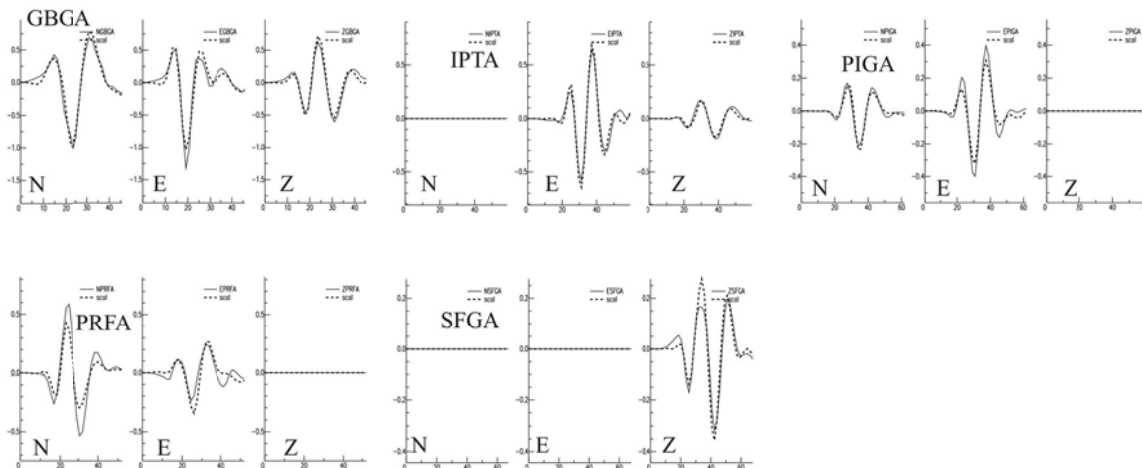


Figure S6. Waveform modeling for the Saintes earthquake. Horizontal axis, time in seconds. Vertical axis, displacement amplitude in centimeters. Continuous line: observed; dashed line: computed. Components where the observed and computed signals are flat correspond to components which were discarded by the inversion.

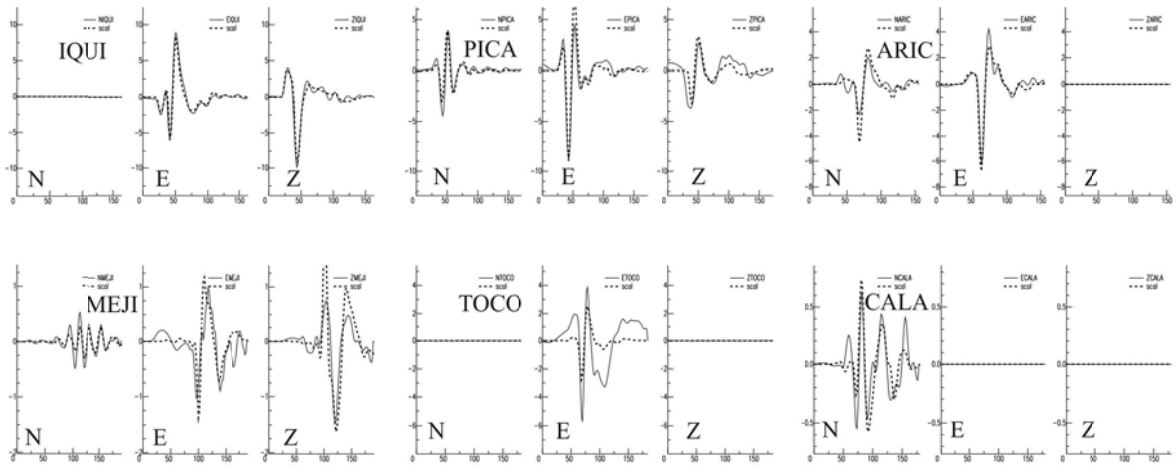


Figure S7. Waveform modeling for the Tarapaca earthquake. Horizontal axis, time in seconds. Vertical axis, displacement amplitude in centimeters. Continuous line: observed; dashed line: computed. Components where the observed and computed signals are flat correspond to components which were discarded by the inversion.

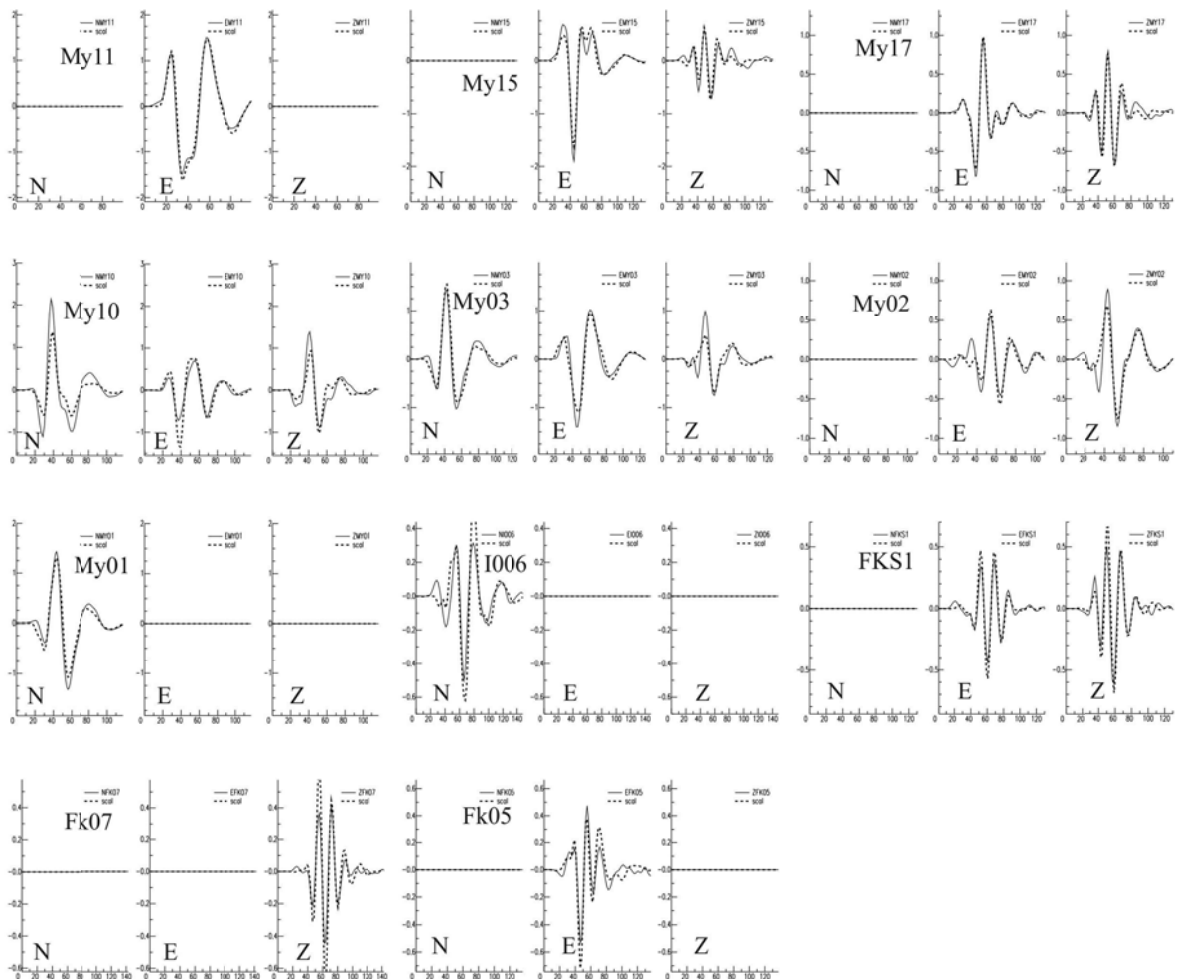


Figure S8. Waveform modeling for the Miyagi-Oki earthquake. Horizontal axis, time in seconds. Vertical axis, displacement amplitude in centimeters. Continuous line: observed; dashed line: computed. Components where the observed and computed signals are flat correspond to components which were discarded by the inversion.

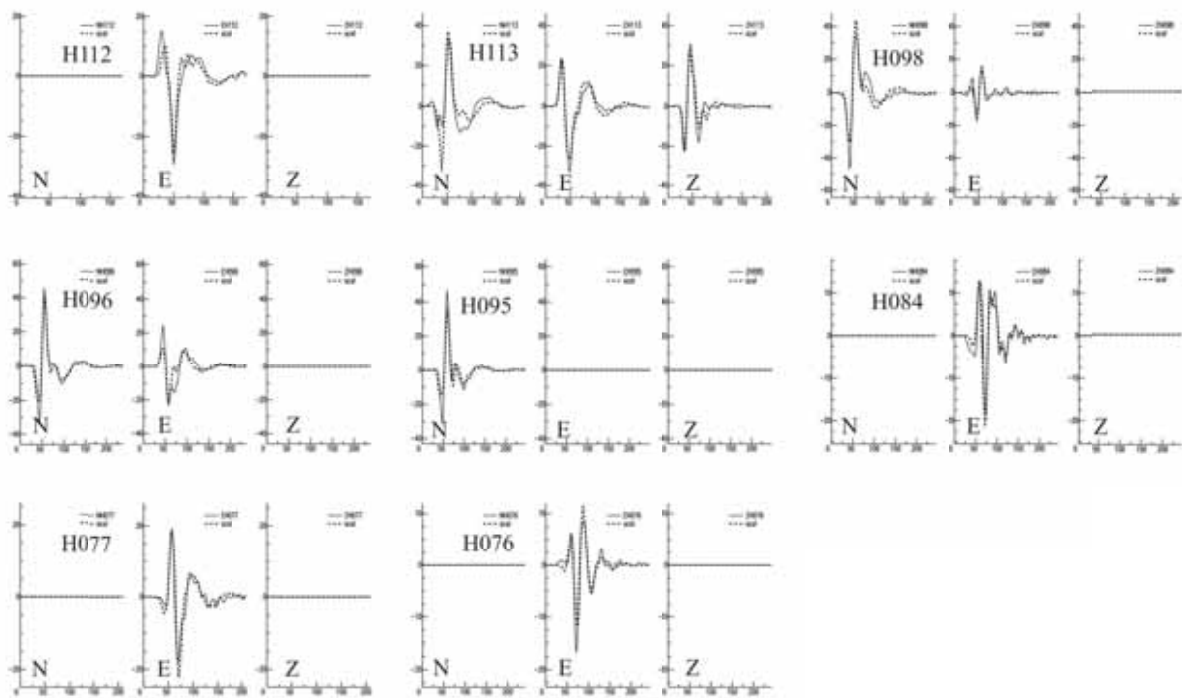
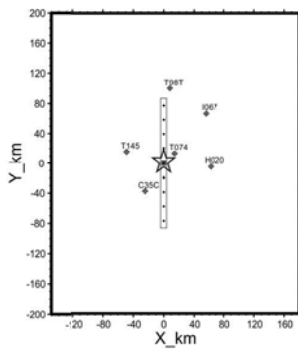
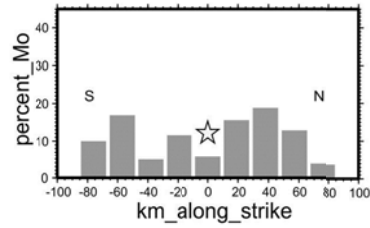


Figure S9. Waveform modeling for the Tokashi-Oki earthquake. Horizontal axis, time in seconds. Vertical axis, displacement amplitude in centimeters. Continuous line: observed; dashed line: computed. Components where the observed and computed signals are flat correspond to components which were discarded by the inversion.

Chichi EQ subset 6 stations #1



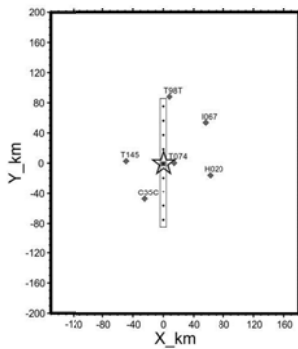
strike dip rake
0. 35. 39.



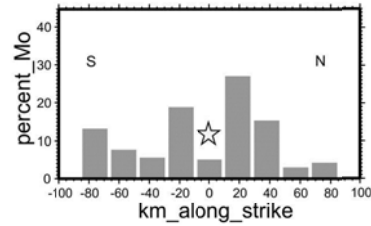
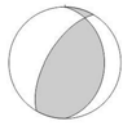
Mw 7.5 Conf Index 82% RMS 0.28 ncomp 15

seismic moment at epicenter: 6%
seismic moment S of epicenter: 43%
seismic moment N of epicenter: 51%

Chichi EQ subset 6 stations #1 Epic displaced 10 km northward



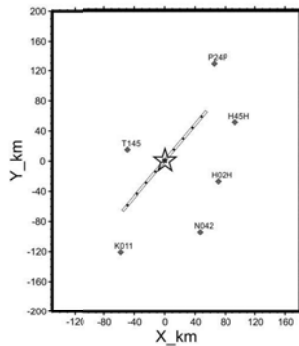
strike dip rake
0. 30. 63.



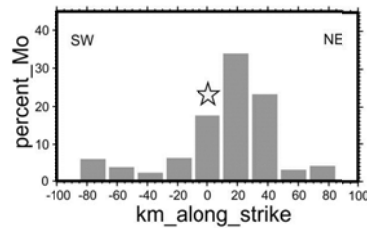
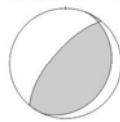
Mw 7.5 Conf Index 78% RMS 0.48 ncomp 14

seismic moment at epicenter: 5%
seismic moment S of epicenter: 45%
seismic moment N of epicenter: 50%

Chichi EQ subset 6 stations #2



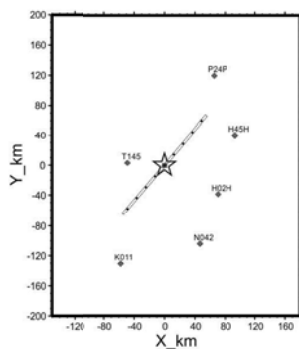
strike dip rake
220. 70. 96.



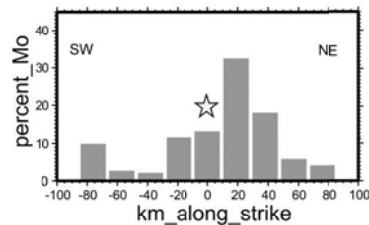
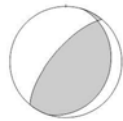
Mw 7.5 Conf Index 78% RMS 0.48 ncomp 14

seismic moment at epicenter: 18%
seismic moment NE of epicenter: 64%
seismic moment SW of epicenter: 18%

Chichi EQ subset 6 stations #2 Epic displaced 10 km northward



strike dip rake
220. 70. 98.



Mw 7.6 Conf Index 80% RMS 0.44 ncomp 13

seismic moment at epicenter: 13%
seismic moment NE of epicenter: 60%
seismic moment SW of epicenter: 26%

Figure S10. Sensitivity tests in the case of the Chichi earthquake. Inversions with two different subsets of 6 stations (#1 and #2), with the original epicenter or the epicenter displaced 10 km northward.

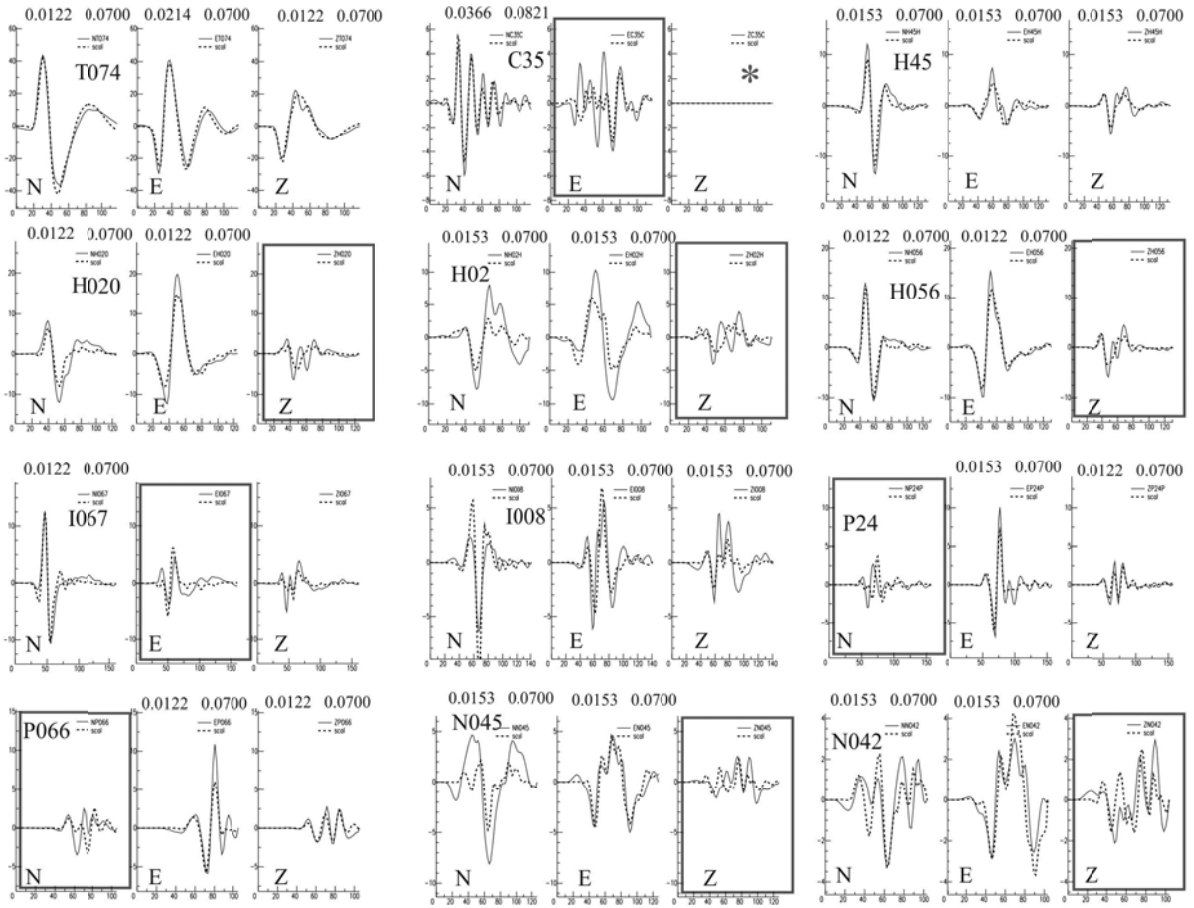


Figure S11. Waveform fit for the Chichi earthquake for a FMNEAR inversion in which the elimination of components as a function of waveform fit is disabled. Components which were discarded by the standard FMNEAR inversion (see Figure 5 of the paper) are indicated by a rectangular frame. The vertical component of C35 marked by a “*” was eliminated during data processing (no bandpass filtering found).

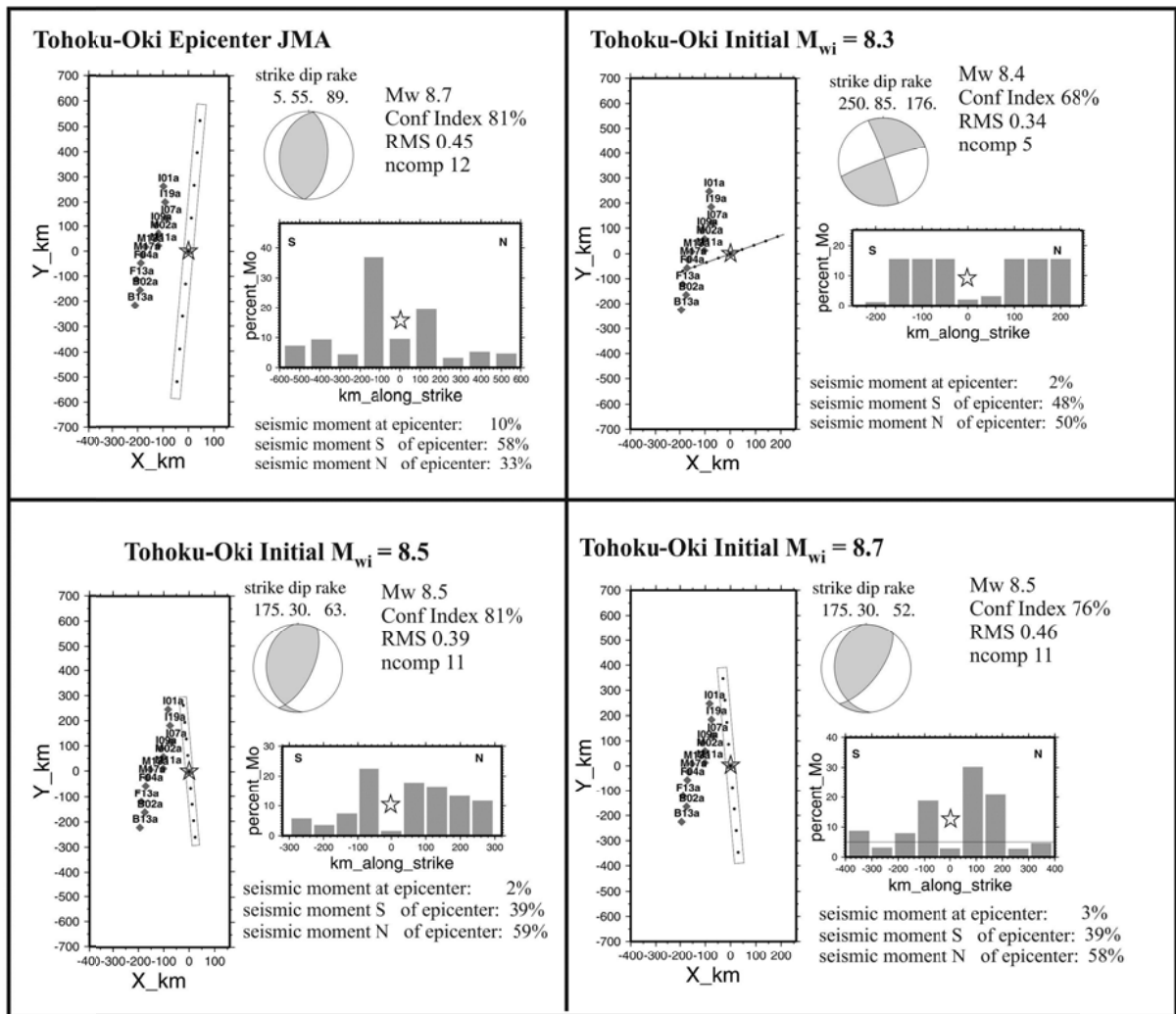


Figure S12. Sensitivity tests in the case of the Tohoku-Oki earthquake. Top left: inversion with the JMA epicenter. Top right: inversion with initial moment magnitude 8.3. Bottom left: inversion with initial moment magnitude 8.5. Bottom right: inversion with initial moment magnitude 8.7.

Tables

Table S1. Velocity models used in the FMNEAR inversions for the different test cases.

	thickness (km)	Vp (km/s)	Vs (km/s)	density (g/cm ³)	Qp	Qs
Chichi and Chengkung *	2.00	3.50	1.966	2.05	250.00	125.00
	2.00	4.40	2.566	2.25	340.00	170.00
	5.00	5.25	3.035	2.45	480.00	240.00
	4.00	6.05	3.457	2.60	550.00	275.00
	4.00	6.36	3.655	2.65	580.00	290.00
	8.00	6.66	3.850	2.70	620.00	310.00
	5.00	7.14	4.103	2.90	680.00	340.00
	5.00	7.43	4.270	3.00	720.00	360.00

	35.00	7.83	4.517	3.10	900.00	450.00	
	0.00	8.10	4.629	3.40	1000.00	500.00	
Tottori †	2.00	5.50	3.18	2.60	500.00	200.00	
	14.00	6.05	3.48	2.70	500.00	200.00	
	22.00	6.60	3.82	2.80	500.00	200.00	
	0.00	8.03	4.62	3.10	1000.00	500.00	
Aquila‡	0.60	3.30	1.90	2.00	200.00	100.00	
	1.40	4.50	2.60	2.30	350.00	175.00	
	3.00	5.50	3.18	2.50	500.00	250.00	
	25.00	6.50	3.75	2.90	600.00	300.00	
	0.00	8.10	4.68	3.30	1000.00	500.00	
Saintes §	3.50	3.50	1.99	2.00	200.00	100.00	
	12.00	6.00	3.41	2.70	500.00	250.00	
	15.00	7.00	3.98	3.00	600.00	300.00	
	0.00	8.00	4.62	3.30	1000.00	500.00	
Tarapaca - Tocopilla !!	1.50	2.80	1.59	1.90	150.00	75.00	1
	5.00	5.80	3.33	2.65	500.00	250.00	
	5.00	6.10	3.51	2.70	550.00	275.00	
	10.00	6.60	3.79	2.90	600.00	300.00	
	20.00	7.10	4.08	3.10	700.00	350.00	
	30.00	7.50	4.31	3.20	900.00	450.00	
	150.00	8.00	4.60	3.30	1000.00	500.00	
	0.00	8.00	4.60	3.30	1000.00	500.00	
Miyagi-Oki and Tohoku 2	3.00	5.50	3.14	2.30	600.00	300.	
	15.00	6.00	3.55	2.40	600.00	300.	
	15.00	6.70	3.83	2.80	600.00	300.	
	67.00	7.80	4.46	3.20	600.00	300.	
	0.00	8.00	4.57	3.30	600.00	300.	
Tokashi-Oki 3	4.00	5.50	3.18	2.60	500.00	250.00	
	10.00	5.80	3.34	2.70	500.00	250.00	
	10.00	6.50	3.74	2.90	600.00	300.00	
	0.00	7.80	4.50	3.20	1200.00	600.00	
Near-Lourdes 4	1.00	5.50	3.14	2.50	500.00	250.00	
	3.00	5.60	3.20	2.55	500.00	250.00	
	7.00	6.10	3.49	2.55	500.00	250.00	
	23.00	6.40	3.66	2.90	600.00	300.00	
	0.00	8.00	4.62	3.30	1000.00	500.00	

* reference: model used by BATS

<http://bats.earth.sinica.edu.tw>

† reference: Semanne et al. (2005)

‡ no reference, kind of standard model
§ reference: Bazin et al. (2010)
!! reference: Delouis and Legrand (2009) and Delouis et al. (2009)
1 for stations IQUI and MEJI only
2 reference: Fukuyama et al. (1998) and in Lee et al. (2011)
3 Reference: Yagi (2004)
4 reference: OMP Toulouse (model used to locale local seismicity in the Pyrenees)

References

Bazin S., N. Feuillet, C. Duclos, W. Crawford, A. Nercessian, M. Bengoubou-Valerius, F. Beauducel, S.C. Singh, 2010. Seismicity and tomographic modelling of Les Saintes (FWI) seismic sequence using ocean bottom seismometers, *Tectonophysics*, 489:1-4, 91-103

Delouis, B. and D. Legrand, 1999. Focal mechanism determination and identification of the fault plane of earthquakes using only one or two near-source seismic recordings. *Seismological Society of America Bulletin* 89, 1558–1574.

Delouis, B., M. Pardo, D. Legrand, and T. Monfret (2009b). The Mw 7.7 Tocopilla earthquake of 14 November 2007 at the southern edge of the northern Chile seismic Gap: Rupture in the deep part of the coupled plate interface, *Bull. Seism. Soc. Am.*, 99, 87-94, doi: 10.1785/0120080192.

Lee, S.-J., B.-S. Huang, M. Ando, H.-C. Chiu, and J.-H. Wang (2011), Evidence of large scale repeating slip during the 2011 Tohoku-Oki earthquake, *Geophys. Res. Lett.*, 38, L19306, doi:10.1029/2011GL049580.

Fukuyama, E., M. Ishida, D. S. Dreger and H. Kawai (1998), Automated seismic moment tensor determination by using on-line broadband seismic waveforms, *Zisin*, 149-156 (in Japanese with English abstract).

Semmane, F., F Cotton, and. M Campillo (2005). The 2000 Tottori earthquake: A shallow earthquake with no surface rupture and slip properties controlled by depth – *J. Geophys. Res.*, vol. 110, B03306, doi:10.1029/2004JB003194

Yagi, Y. (2004). Source rupture process of the 2003 Tokachi-oki earthquake determined by joint inversion of teleseismic body wave and strong ground motion data, *Earth Planets Space*, 56, 311-316.